

Article

# Coactivation of GSK3 $\beta$ and IGF-1 Attenuates Amyotrophic Lateral Sclerosis Nerve Fiber Cytopathies in SOD1 Mutant Patient-Derived Motor Neurons

Hsiao-Chien Ting <sup>1,†</sup>, Hui-I Yang <sup>1,2,†</sup>, Horng-Jyh Harn <sup>1,3</sup>, Ing-Ming Chiu <sup>4</sup> , Hong-Lin Su <sup>5</sup>, Xiang Li <sup>6</sup>, Mei-Fang Chen <sup>7</sup>, Tsung-Jung Ho <sup>2,8,9,10</sup>, Ching-Ann Liu <sup>1,7,11</sup>, Yung-Jen Tsai <sup>1</sup>, Tzyy-Wen Chiou <sup>12</sup>, Shinn-Zong Lin <sup>1,2,13,\*</sup> and Chia-Yu Chang <sup>1,7,11,\*</sup> 

- <sup>1</sup> Bioinnovation Center, Buddhist Tzu Chi Medical Foundation, Hualien 97002, Taiwan; sharkzoe@yahoo.com.tw (H.-C.T.); s8706083@yahoo.com.tw (H.-I.Y.); arthewduke@gmail.com (H.-J.H.); sagianne@gmail.com (C.-A.L.); cljbalaa@gmail.com (Y.-J.T.)
- <sup>2</sup> Institute of Medical Sciences, Tzu Chi University, Hualien 97004, Taiwan; jeron888@gmail.com
- <sup>3</sup> Department of Pathology, Hualien Tzu Chi Hospital and Tzu Chi University, Hualien 97002, Taiwan
- <sup>4</sup> Institute of Cellular and System Medicine, National Health Research Institutes, Miaoli 35053, Taiwan; ingming@nhri.edu.tw
- <sup>5</sup> Department of Life Sciences, National Chung Hsing University, Taichung 40227, Taiwan; suhonglin@gmail.com
- <sup>6</sup> Waisman Center, University of Wisconsin, Madison, WI 53705, USA; michael2025li@163.com
- <sup>7</sup> Department of Medical Research, Hualien Tzu Chi Hospital, Hualien 97002, Taiwan; mfcchen@mail.tcu.edu.tw
- <sup>8</sup> Department of Chinese Medicine, Hualien Tzu Chi Hospital, Hualien 97002, Taiwan
- <sup>9</sup> Integration Center of Traditional Chinese and Modern Medicine, Hualien Tzu Chi Hospital, Hualien 97002, Taiwan
- <sup>10</sup> School of Post-Baccalaureate Chinese Medicine, Tzu Chi University, Hualien 97004, Taiwan
- <sup>11</sup> Neuroscience Center, Hualien Tzu Chi Hospital, Hualien 97002, Taiwan
- <sup>12</sup> Department of Life Science, National Dong Hwa University, Hualien 97441, Taiwan; twchiou@gms.ndhu.edu.tw
- <sup>13</sup> Department of Neurosurgery, Hualien Tzu Chi Hospital, Hualien 97002, Taiwan
- \* Correspondence: shinnzong@yahoo.com.tw (S.-Z.L.); scata0726@hotmail.com (C.-Y.C.); Tel.: +886-3-856-1825 (ext. 13201) (S.-Z.L.); +886-3-856-1825 (ext. 12106) (C.-Y.C.)
- † Co-first authors.



**Citation:** Ting, H.-C.; Yang, H.-I.; Harn, H.-J.; Chiu, I.-M.; Su, H.-L.; Li, X.; Chen, M.-F.; Ho, T.-J.; Liu, C.-A.; Tsai, Y.-J.; et al. Coactivation of GSK3 $\beta$  and IGF-1 Attenuates Amyotrophic Lateral Sclerosis Nerve Fiber Cytopathies in SOD1 Mutant Patient-Derived Motor Neurons. *Cells* **2021**, *10*, 2773. <https://doi.org/10.3390/cells10102773>

Academic Editor: Andrea Pession

Received: 16 September 2021

Accepted: 14 October 2021

Published: 16 October 2021

**Publisher's Note:** MDPI stays neutral with regard to jurisdictional claims in published maps and institutional affiliations.



**Copyright:** © 2021 by the authors. Licensee MDPI, Basel, Switzerland. This article is an open access article distributed under the terms and conditions of the Creative Commons Attribution (CC BY) license (<https://creativecommons.org/licenses/by/4.0/>).

**Abstract:** Amyotrophic lateral sclerosis (ALS) is a progressive nervous system disease that causes motor neuron (MN) degeneration and results in patient death within a few years. To recapitulate the cytopathies of ALS patients' MNs, *SOD1*<sup>G85R</sup> mutant and corrected *SOD1*<sup>G85G</sup> isogenic-induced pluripotent stem cell (iPSC) lines were established. Two *SOD1* mutant ALS (*SOD1*<sup>G85R</sup> and *SOD1*<sup>D90A</sup>), two *SOD1* mutant corrected (*SOD1*<sup>G85G</sup> and *SOD1*<sup>D90D</sup>), and one sporadic ALS iPSC lines were directed toward MNs. After receiving ~90% purity for MNs, we first demonstrated that *SOD1*<sup>G85R</sup> mutant ALS MNs recapitulated ALS-specific nerve fiber aggregates, similar to *SOD1*<sup>D90A</sup> ALS MNs in a previous study. Moreover, we found that both *SOD1* mutant MNs showed ALS-specific neurite degenerations and neurotransmitter-induced calcium hyperresponsiveness. In a small compound test using these MNs, we demonstrated that gastrodin, a major ingredient of *Gastrodia elata*, showed therapeutic effects that decreased nerve fiber cytopathies and reverse neurotransmitter-induced hyperresponsiveness. The therapeutic effects of gastrodin applied not only to *SOD1* ALS MNs but also to sporadic ALS MNs and *SOD1*<sup>G93A</sup> ALS mice. Moreover, we found that coactivation of the GSK3 $\beta$  and IGF-1 pathways was a mechanism involved in the therapeutic effects of gastrodin. Thus, the coordination of compounds that activate these two mechanisms could reduce nerve fiber cytopathies in *SOD1* ALS MNs. Interestingly, the therapeutic role of GSK3 $\beta$  activation on *SOD1* ALS MNs in the present study was in contrast to the role previously reported in research using cell line- or transgenic animal-based models. In conclusion, we identified in vitro ALS-specific nerve fiber and neurofunctional markers in MNs, which will be useful for drug screening, and we used an iPSC-based model to reveal novel therapeutic mechanisms (including GSK3 $\beta$  and IGF-1 activation) that may serve as potential targets for ALS therapy.

**Keywords:** amyotrophic lateral sclerosis (ALS); induced pluripotent stem cell (iPSC); motor neuron (MN); *SOD1*; drug screening; gastrodin; GSK3 $\beta$ ; IGF-1

## 1. Introduction

Amyotrophic lateral sclerosis (ALS) is one of the most serious motor neuron (MN) degenerative diseases: It has an incidence of five to six cases per million people and an effective treatment is not currently available. ALS patients suffer from motor function degeneration from the body terminals; within 3–5 years, patients lose most of their motor function and finally die from respiratory failure [1]. Current FDA-approved ALS treatment drugs, including riluzole, edaravone, and Nuedexta, which show limited therapeutic effects on ALS patients [2–4].

Most ALS cases are sporadic with unknown causes, whereas 10–20% are from pathogenic genetic mutations. Known mutations of genes such as *SOD1* [5,6], *ALS2* [7], *TARDBP* [8,9], *C9orf72* [10], *FUS* [11,12], *OPTN* [13], and *VAPB* [14] induce familial or early-onset ALS. About 20% of familial ALS cases are caused by *SOD1* mutations [5,6].

The clinical pathology of ALS includes mutated pathogenic protein accumulation, nerve fiber degeneration, and MN functional loss [15,16]. Other cytopathies, including endoplasmic reticulum stress, mitochondrial dysfunction, and high-level reactive oxygen species, have been identified in various ALS in vitro and animal models [17–19]. These MN cytopathies can lead to the disruption of neuron–neuron and neuromuscular junctions.

Although transgenic cell lines and animals have been used in ALS research for decades, huge gaps still exist between current laboratory models and human patients. Most models have been generated from immortalized cell lines or animals with high-level expression of human ALS pathogenic transgenes [20,21]. Thus, these models may have ALS like late-stage outcomes but dissimilar disease mechanisms compare with those of real patients. To recapitulate the cytopathies of patients, patient cell-derived induced pluripotent stem cells (iPSCs) are now applied in ALS in vitro modeling. Neurite length decrease, protein aggregates, oxidative stress, mitochondrial dysfunction, and cell apoptosis have all been observed in non-*SOD1* ALS MNs [22–33]. *SOD1* mutation MNs express *SOD1* aggregates and neurofilament dysregulation phenotypes [27]. Until now, two potential compounds, Src/c-Abl inhibitor and ropinirole, have been screened from ALS iPSC-based models and are under clinical development [26,32]. However, ropinirole exhibits no significant effects on *SOD1*-type ALS MNs [32]. Therefore, the disease mechanisms and candidate therapeutic targets of *SOD1* and sporadic ALS must still be elucidated.

In the present study, we applied a CHSF-based differentiation method (a neural differentiation protocol with CHIR99021, SB431542, and FGF-basic) for efficient generation of high-purity *SOD1* ALS MNs. The novel paradigmatic nerve fibers and functional cytopathology of ALS were observed in *SOD1* ALS iPSCs but not in corrected healthy iPSC-derived MNs within 28–38 days of differentiation. Gastrodin, a natural small compound screened from this model, was able to reduce nerve fiber and neurofunctional cytopathies, while also providing therapeutic effects on sporadic ALS MNs and transgenic mice. IGF-1 and GSK3 $\beta$  activation were the major therapeutic mechanisms of gastrodin treatment and also significantly reduced ALS phenotypes. Interestingly, the role of GSK3 $\beta$  in ALS reported here is opposed to that previously reported in earlier transgenic model-based studies.

## 2. Materials and Methods

### 2.1. iPSC Line Establishment and Culture

The *SOD1*<sup>D90A</sup> and *SOD1*<sup>D90D</sup> iPSC lines were purchased from WiCell (Madison, WI, USA). *SOD1*<sup>G85R</sup> and sporadic ALS iPSC lines were generated from patients' PBMCs with the approval of the Ethic Institutional Review Board in Hualien Tzu Chi Hospital (IRB105-131-A). Informed consent was obtained from patients. Patients' PBMCs were cultured in StemPro 34 SFM (ThermoFisher Scientific, Waltham, MA, USA) supplemented with SCF,

FLT-3, IL-3, and IL-6 (all Peprotech, Cranbury, NJ, USA). Reprogramming was processed with a CytoTune iPS 2.0 Sendai Reprogramming Kit [34] (ThermoFisher Scientific) according to the kit manual. Emerging colonies were transferred to 1% Geltrex (ThermoFisher Scientific)-coated culture dishes and expanded in TeSR-E8 medium (StemCell Technologies, Vancouver, BC, Canada) or Pluto human iPS/ES cell culture medium (DuoGenic Stem Cells, Taichung, Taiwan). The iPSCs were passaged for 3–5 days with Accutase (Merck-Millipore, Billerica, MA, USA) and then reseeded at 1:5 to 1:10 ratios. Culture media were refreshed daily.

### 2.2. *SOD1<sup>G85R</sup> iPSC Site-Specific Correction by CRISPR/Cas9-Mediated Homologous Recombination*

*SOD1<sup>G85R</sup>* mutation correction was processed by Applied StemCell (Milpitas, CA, USA). Briefly, gRNAs were designed near exon 4 of *SOD1* and the site-specific cutting efficiency was identified with a surveyor nuclease assay. A 200-nt single-stranded DNA oligonucleotide homologous arm around the *SOD1* G256C mutated site was delivered together with Cas9/sgRNA plasmid by nucleofection. Emerging colonies were individually collected and the *SOD1* G256 site was analyzed by DNA sequencing. Two clones, A7 and A9, were identified with corrected G256G sites. The *SOD1<sup>G85G</sup>* iPSC line used in this study was the A7 clone.

### 2.3. *Robust MN Differentiation from iPSCs*

While the iPSCs reached 80% confluence in a culture dish, the cells were treated with 1 mg/mL of Dispase II (Sigma-Aldrich, Saint Louis, MO, USA) for 5–15 min until the periphery of colonies started to become rounded up; they were then lifted by scraping. The cell clumps were dissociated into 200–300 µm clusters and transferred into ultra-low attachment dishes in TeSR-E6 medium (StemCell Technologies) for 1 day to form embryoid bodies (EBs). Additionally, 5 µM of Y27632 (Cayman Chemical, Ann Arbor, MI, USA) was added during the first 4 h to avoid iPSC blebbing. The EBs were subjected to the CHSF neural epithelial induction method. The neural induction medium comprised DMEM-F12 basal medium supplied with 1% N2 supplement, 1 mM of NEAAs, and 2 mM of glutamate (all ThermoFisher Scientific). CHSF factors, including 3-µM CHIR99021 (Cayman Chemical), 10-µM SB431542 (Sigma-Aldrich), and 10-ng/mL recombinant human FGF-2 (rh-FGF2; R&D Systems, Minneapolis, MN, USA) were added on days 1–4. On day 4, the neural induction medium was changed to neurobasal medium (ThermoFisher Scientific) with 1% N2 supplement, 1-mM NEAAs, 2-mM glutamate, and MN patterning factors, including 3 µM of CHIR99021, 2 µM of SB431542, 200 nM of LDN193189 (Cayman Chemical), 0.5 µM of SAG (Cayman Chemical), and 0.5 µM of retinoic acid (Sigma-Aldrich), until day 14 of differentiation. Both 0.5 µM SAG and 0.5 µM retinoic acid were continually added until day 25 of differentiation. According to EB condition, 2% B27 supplement (ThermoFisher Scientific) was potentially added to the culture medium and the EBs were moved to cell culture flasks or dishes on day 15. Before experimental assays, the EBs were dissociated into small clumps using Accutase and seeded on 1% Geltrex-coated cell culture dishes supplemented with 0.2 µM of compound E (Cayman Chemical) but without BDNF, GDNF, or dbcAMP. The addition of neurotrophic factors can delay or eliminate the ALS nerve fiber cytopathies in iPSC-derived MNs. In the first 4 h of cell adhesion, 1% RevitaCell supplement (ThermoFisher Scientific) was added to the cells.

### 2.4. *Immunocytochemistry (ICC) Staining and Nerve Fiber Density/Beads Calculations*

First, iPSCs and differentiated cells were seeded in 24-well plates and fixed with 4% paraformaldehyde (Sigma-Aldrich) at room temperature; then, they were washed twice with phosphate-buffered saline (PBS). Cells were permeabilized with 0.1% Triton-100 for 15 min at 4 °C and then blocked with 5% horse serum. Primary antibodies were incubated with cells at 4 °C for 16 h, washed twice, and then conjugated with secondary antibodies. The primary antibodies used in this study included those against Oct-4 (1:200), Brachyury

(1:50), N-cadherin (1:500), and Sox-1 (1:200) (all Santa Cruz Biotechnology); Nanog (1:30) and Sox-17 (1:20) (both R&D systems); Pax-6 (1:100), Nestin (1:500), and  $\beta$ III-tubulin (1:500) (all Covance, Princeton, NJ, USA); NF (1:500), phosphorylated neurofilament H & M (1:500), and choline acetyltransferase (1:100) (all Sigma-Aldrich); and Sox-2 (1:200; GeneTex, Irvine, CA, USA), SSEA-4 (1:100; BD Pharmingen, Franklin Lakes, NJ, USA), Islet-1 (1:500; NeuroMics, Edina, MN, USA), Oligo-2 (1:500; Novus Biologicals, Centennial, CO, USA), and HB9/MNX1 (1:50; Developmental Studies Hybridoma Bank, DSHB, Iowa City, IA, USA). Cell nuclei were stained with diamidino-2-phenylindole (DAPI). Fluorescence images were captured using an upright microscope (Imager Z1, Zeiss, Oberkochen, Germany). Neurite density and nerve fiber beads were calculated with Olympus CellSens Dimension Desktop 3.1 (Olympus Corporation, Tokyo, Japan) using the images from three independent experiments.

### 2.5. Calcium Imaging

Cells were seeded on Geltrex-coated 10-mm cover slides and cultured in physiological buffer with 1  $\mu$ M of Fluo-4 at 37 °C for 40 min. Subsequently, they were incubated in physiological buffer (including 30 mM of NaCl, 5 mM of KCl, 2 mM of CaCl<sub>2</sub>, 2 mM of MgCl<sub>2</sub>, 10 mM of glucose, and 10 mM of HEPES) for 20 min. The cells were then moved to a calcium imaging chamber, washed with physiological buffer for 30 s, and treated with 60 mM of KCl for 60 s. After a 5 min wash in physiological buffer, the cells were treated with 1 mM of L-glutamate for 60 s. Images were taken with an ECLIPSE Ti2-E microscope (Nikon, Tokyo, Japan) and analyzed with NIS-Elements AR (Nikon).

### 2.6. ALS Animal Model and Small Compound Treatment

Transgenic mice overexpressing the human *SOD1*<sup>G93A</sup> mutation (*SOD1*-G93A-1Gur/J) were purchased from Jackson Laboratory (Bar Harbor, ME, USA) and used in this study. All animal-related procedures were performed in accordance with the guidelines of the US National Institutes of Health and Hualien Tzu Chi Hospital (106-46), Taiwan. Mice were separated into three groups at 60 days of age: (1) vehicle control, (2) 50 mg/kg body weight of gastrodin, and (3) 200 mg/kg body weight of gastrodin. They were treated with vehicle or gastrodin by intraperitoneal injection five times per 30 days within the individual animal's lifespan.

### 2.7. Animal Motor Behavior Test

Motor function of ALS mice was measured using the BBB scale, grip strength test, and rotarod test. BBB scale measurements began at 90 days of age and continued within the individual animal's lifespan. Briefly, mice were free to walk around their cage and were observed for ~3–5 min. The hindlimb score was based on a 21 to 0-point scoring range from normal to no movement as measured by tail elevation, paw position, sweeping without weight bearing, movement of the hindlimb joints, forelimb–hindlimb step, consistent weight support, and frequent plantar stepping [35]. In the grip strength test, mice were placed on a grid and the base of their tail was pulled in the opposite direction to record their grip power. In the rotarod test, before 90 days of age, mice were placed on a rotating rod that turned at 5 rpm for 300 s for training. After 90 days of age, mouse data were collected by rotating the rod at 5 rpm on average with an acceleration of 0–30 rpm.

### 2.8. Western Blotting

Cells were lysed in a 200- $\mu$ L lysis buffer composed of M-PER, 1% phosphatase protease inhibitor, and 50 mM of EDTA; subsequently, they were centrifuged at 14,000 rpm and 4 °C for 15 min. Protein concentrations were determined using the Bradford assay (Bio-Rad Laboratories, Hercules, CA, USA). Purified proteins (15 mg) were subjected to SDS-PAGE, transferred to PVDF membranes, blocked with 5% skim milk for 1 h, and then probed with primary antibodies against GAPDH (1:10000), p44/42 MAPK (1:1000), phospho-p44/42 MAPK (Thr202/Tyr204) (1:1000), MEK1/2 (1:1000), phospho-MEK1/2

(Ser217/221) (1:1000), Akt (pan) (1:1000), phospho-Akt (Ser473) (1:2000) (all Cell Signaling Technology, Danvers, MA, USA), GSK3 $\beta$  (1:3000; ProteinTech, Rosemont, IL, USA), and phospho-GSK3 (Tyr279/Tyr216) (1:500; Sigma-Aldrich) at 4 °C overnight. Membranes were then washed with PBS containing 0.1% Tween-20 before they were incubated with HRP-conjugated secondary antibody at room temperature for 1 h. All proteins were detected using Immobilon Crescendo Western HRP substrate (Millipore) and recorded with FUSION Solo S (Vilber, Collégien, France). The band intensity of Western blotting was quantified with image J (National Institutes of Health) then applied to statistical analysis.

### 2.9. RNA-Microarray and Analysis

An amount of 0.2  $\mu$ g of total RNA was amplified by a Low Input Quick-Amp Labeling kit (Agilent Technologies, Santa Clara, CA, USA) and labeled with Cy3 (CyDye, Agilent Technologies) during the *in vitro* transcription process. Then 0.6  $\mu$ g of Cy3-labeled cRNA was fragmented by incubation with fragmentation buffer at 60 °C for 30 min. Correspondingly fragmented labeled cRNA was then pooled and hybridized to Agilent SurePrint Microarray (Agilent Technologies) at 65 °C for 17 h. After washing and drying by nitrogen gun blowing, microarrays were scanned with an Agilent microarray scanner (Agilent Technologies). Scanned images were analyzed by Feature extraction10.7.3.1 software (Agilent Technologies), an image analysis and normalization software that is used to quantify signal and background intensity for each feature. Raw signal data were normalized by quantile normalization for differential expressed genes discovering. For functional assay, we provided an enrichment test for differential expressed genes (For most model organisms). Welgen Biotech used clusterProfiler for enrichment test for gene ontology (GO) and pathway (KEGG).

### 2.10. Statistical Analysis

Data were collected and analyzed from no less than three independent experimental results and are shown as means  $\pm$  SD. Student's t-test or one-way ANOVA with Tukey's post hoc test were used to test for differences between groups. *p* values < 0.05 were considered statistically significant.

## 3. Results

### 3.1. Generation of *SOD1*<sup>G85R</sup> ALS and *SOD1*<sup>G85G</sup> Isogenic iPSCs, and Robust MN Differentiation via the CHSF Method

We obtained *SOD1*<sup>D90A</sup>- and *SOD1*<sup>D90D</sup>-corrected isogenic iPSC lines from WiCell, which were previously reported by Chen et al. [27]. Additionally, we established *SOD1*<sup>G85R</sup> iPSC lines from the peripheral blood mononuclear cells (PBMCs) of an early-onset ALS patient. G85R was one of the earliest discovered *SOD1* mutant sites in familial ALS [36,37]. After reprogramming and clonal selection, individual iPSC clones became stable lines. One clone (*SOD1*<sup>G85R</sup>) was subjected to iPSC characterization. *SOD1*<sup>G85R</sup> iPSC exhibited classical pluripotent stem cell morphology (Figure 1a) and expressed pluripotent-specific markers including Oct4, Nanog, Sox2, and SSEA-4 (Figure 1d–g). The *SOD1*<sup>G85R</sup> iPSCs obtained normal karyotypes (Figure 1b) and heterogeneous G to C mutations on the *SOD1* 256-nucleic acid site in exon 4 (Figure 1c, upper panel; the G256C mutation was identified with reverse primer sequencing). After *in vitro* differentiation, *SOD1*<sup>G85R</sup> iPSCs could differentiate into cells expressing three germ-layer progenitor cell markers, i.e., ectoderm with Sox1 and N-Cadherin expression (Figure 1h), mesoderm with Brachyury expression (Figure 1i), and endoderm with Sox17 expression (Figure 1j).

For a reliable ALS cytopathy isogenic control, we applied the CRISPR/Cas9 gene editing tool to correct the *SOD1* G256C mutation. The normal *SOD1* sequence near the *SOD1* G256C site was flanked with homologous arms and sgRNAs were delivered into *SOD1*<sup>G85R</sup> iPSCs. After clonal expansion, the *SOD1* G256C site was analyzed by sequencing and one iPSC clone was identified (*SOD1*<sup>G85G</sup>-A7) with a mutant site correction (Figure 1c, lower panel; homogeneous G was identified with reverse primer sequencing).

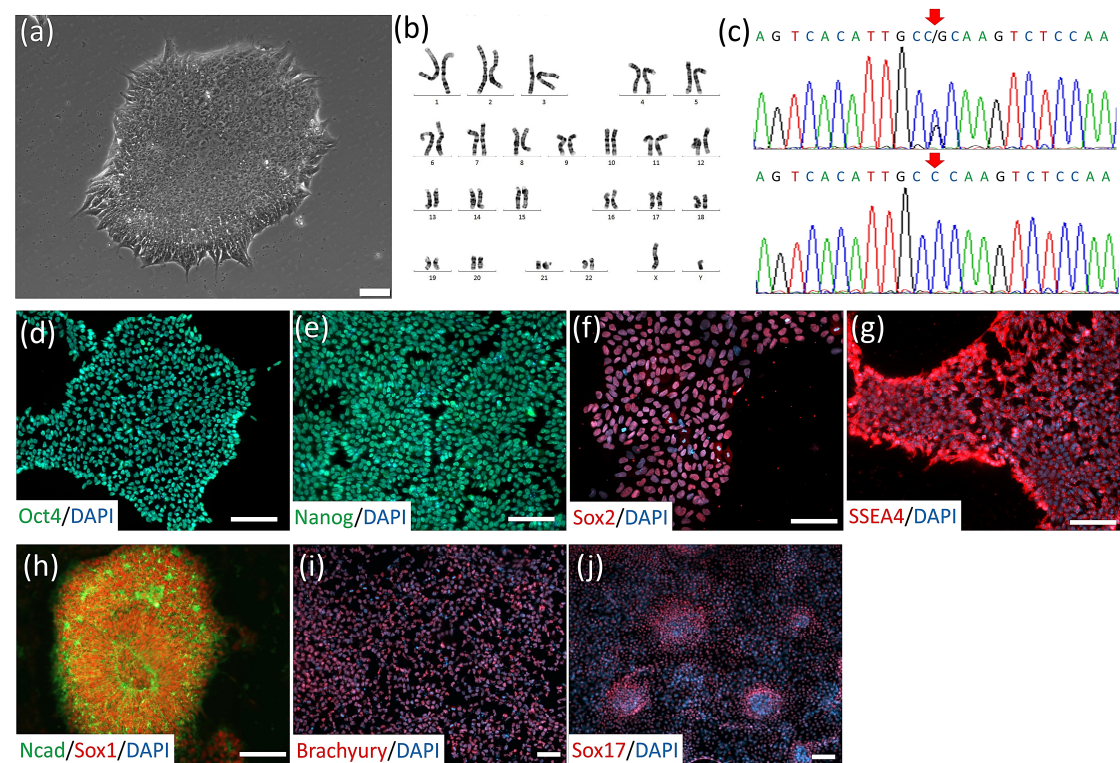


**Figure 1.** iPSC generation and SOD1 mutant site correction. (a) Morphology of *SOD1*<sup>G85R</sup> ALS patient's PBMC-derived iPSC clone. (b) Karyotype of *SOD1*<sup>G85R</sup> iPSCs. (c) DNA sequencing of *SOD1*<sup>G85R</sup> iPSCs (upper panel) and corrected *SOD1*<sup>G85G</sup> iPSCs (lower panel). Mutant and corrected site are emphasized with arrows. (d–g) *SOD1*<sup>G85R</sup> iPSC-expressed pluripotent stem cell-specific markers including Oct-4 (d), Nanog (e), Sox-2 (f), and SSEA4 (g). (h–j) In vitro differentiation of *SOD1*<sup>G85R</sup> iPSCs into cell types with three germ layer cell markers including the ectoderm markers N-cadherin and Sox-1 (h), mesoderm marker Brachyury (i), and endoderm marker Sox-17 (j). Scale bar, 100  $\mu$ m.

Our neural stem cell (NSC) differentiation method was modified from the previously reported BiSF method [38,39]. Specifically, BIO in the BiSF method was replaced with CHIR99021 (a GSK3 $\beta$  inhibitor). After NSC induction, MN patterning factors were added to culturing cells (Figure 2a). At day 15, differentiated cells of four iPSC lines (*SOD1*<sup>G85R</sup>: Figure 2b,c; *SOD1*<sup>G85G</sup>: Figure 2e,f; *SOD1*<sup>D90A</sup>: Figure 2h,i; and *SOD1*<sup>D90D</sup>: Figure 2k,l) expressed the neural stem cell-specific markers Sox1 and N-cadherin as well as the MN progenitor markers Oligo2 or Islet1 in a large number of rosette-like structures. According to the previous publication, the MN progenitor markers Oligo2 or Islet1 might represent the MN fate cells at different MN differentiation stages [40]. Thus, the total cells with the expression of Oligo2 or Islet1 (Figure 2c,f,l,l) presented a high yield of potential MN fate cells at day 15. At days 23–25, differentiated cells expressed neurofilament protein (NF) in nerve fiber-like structures and the MN-specific marker HB9 (also known as MNX1) (*SOD1*<sup>G85R</sup>: Figure 2d; *SOD1*<sup>G85G</sup>: Figure 2g; *SOD1*<sup>D90A</sup>: Figure 2j; and *SOD1*<sup>D90D</sup>: Figure 2m). The expression ratio of HB9 at day 25 was approximately 90–94% of NF<sup>+</sup> cells (*SOD1*<sup>G85R</sup>: 90.95  $\pm$  3.61%; *SOD1*<sup>G85G</sup>: 94.20  $\pm$  1.23%; *SOD1*<sup>D90A</sup>: 94.33  $\pm$  1.53%; *SOD1*<sup>D90D</sup>: 92.93  $\pm$  2.35%) and 86%–91% of total cells (*SOD1*<sup>G85R</sup>: 86.85  $\pm$  4.88%; *SOD1*<sup>G85G</sup>: 89.47  $\pm$  2.61%; *SOD1*<sup>D90A</sup>: 89.90  $\pm$  2.69%; *SOD1*<sup>D90D</sup>: 91.33  $\pm$  2.04%) (Figure 2n) in each line. These data suggest that the *SOD1* mutant and corrected iPSC lines did not have a significant effect on MN differentiation ability.

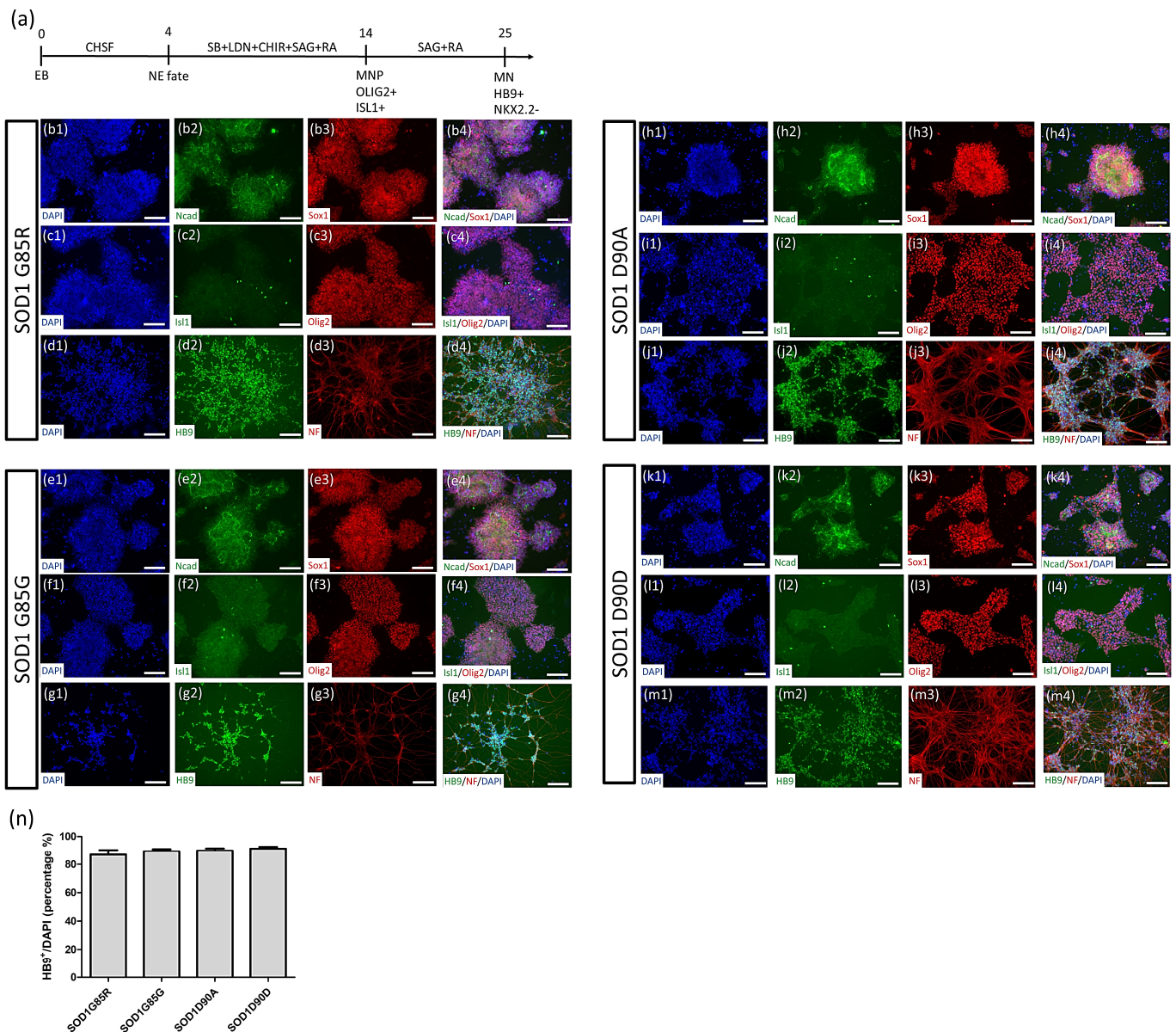


**Figure 2.** Robust generation of MNs from iPSCs. (a) Procedure for CHSF-based MN differentiation. (b–m) Identification of *SOD1*<sup>G85R</sup> (b–d), *SOD1*<sup>G85G</sup> (e–g), *SOD1*<sup>D90A</sup> (h–j), and *SOD1*<sup>D90D</sup> (k–m) iPSC line-derived MN progenitors and MNs. Every line was identified with neural stem cell markers (N-cadherin and Sox-1) and MN progenitor markers (Oligo-2 and Islet-1) at day 15 of differentiation, and with an MN marker (HB9) and a neuronal marker (NF) at days 23–25 of differentiation. (n) Calculation of the HB9 expression ratio of DAPI<sup>+</sup> cells. Scale bar, 100  $\mu$ m.

### 3.2. NF Aggregates and Nerve Fiber Degeneration in *SOD1* ALS MNs

NF inclusions in the MNs of ALS patient tissue have previously been identified; NF inclusions in *SOD1*<sup>D90A</sup> and *SOD1*<sup>A4V</sup> MNs were first discovered by Chen et al. [27]. In the present study, we found NF inclusions in *SOD1*<sup>G85R</sup> MNs in somas and bead-like aggregates on neurites ( $211.4 \pm 47.11$  beads/ $5 \times 10^5$  pixels<sup>2</sup> NF) (Figure 3a) but not in the *SOD1*<sup>G85G</sup> control ( $18.23 \pm 1.13$  beads/ $5 \times 10^5$  pixels<sup>2</sup> NF) (Figure 3c; calculated as Figure 3e), similar to the findings for *SOD1*<sup>D90A</sup> MNs (*SOD1*<sup>D90A</sup>:  $163.3 \pm 12.70$  beads/ $5 \times 10^5$  pixels<sup>2</sup> NF; *SOD1*<sup>D90D</sup>:  $41.92 \pm 7.76$  beads/ $5 \times 10^5$  pixels<sup>2</sup> NF) (Figure 3g,i,k). For the non-MN control, the Shh agonist SAG was replaced with the antagonist cyclopamine to generate neuron types in the dorsal spinal cord; no obvious NF inclusions were observed in *SOD1*<sup>G85R</sup> and *SOD1*<sup>D90A</sup> non-MNs (data not shown).

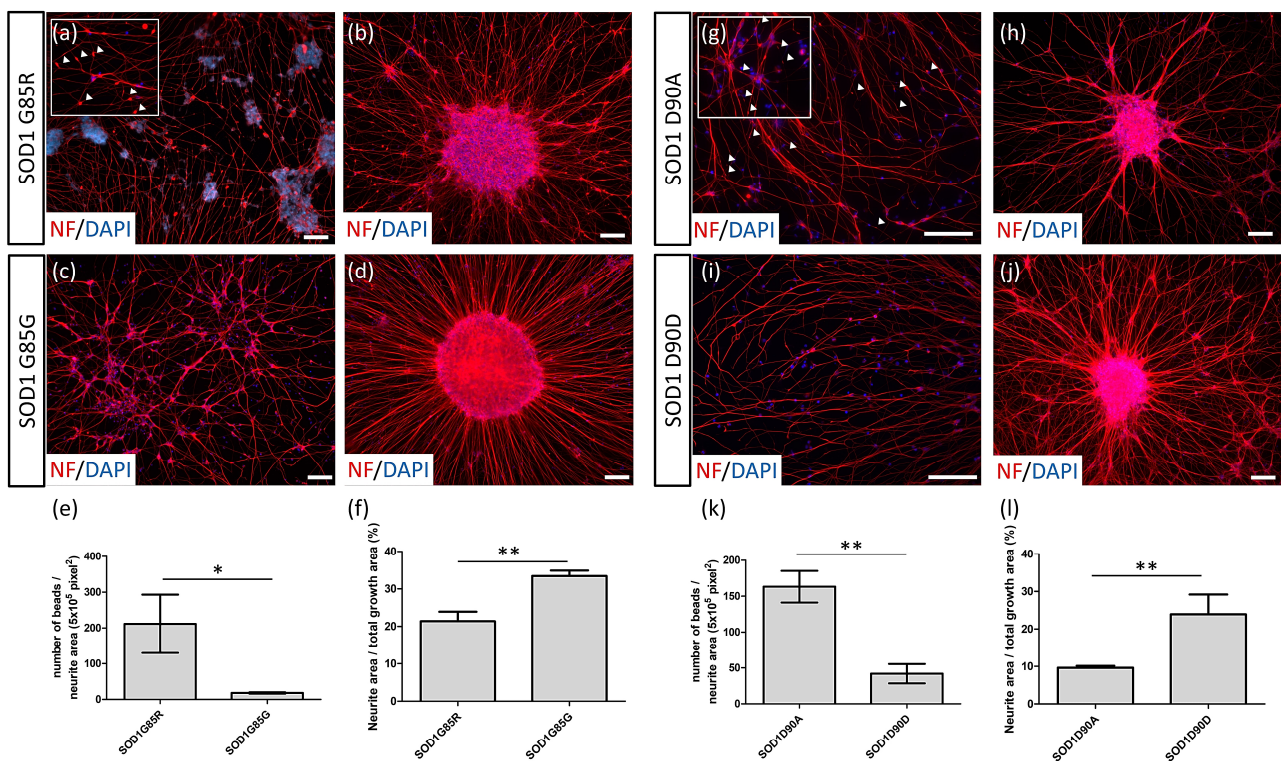


**Figure 3.** Nerve fiber beads and neurite degeneration in SOD1 ALS MNs. (a–d) Nerve fiber beads (a) and neurite density (b) of *SOD1*<sup>G85R</sup> and *SOD1*<sup>G85G</sup> (nerve fiber beads: c; neurite density: d) MNs identified with NF immunocytochemistry staining. (e) Number of nerve fiber beads of *SOD1*<sup>G85R</sup> and *SOD1*<sup>G85G</sup> MNs at day 35 of differentiation. (f) Neurite density of *SOD1*<sup>G85R</sup> and *SOD1*<sup>G85G</sup> MNs at day 28 of differentiation. (g–j) Nerve fiber beads (g) and neurite density (h) of *SOD1*<sup>D90A</sup> and *SOD1*<sup>D90D</sup> (nerve fiber beads: (i); neurite density: (j)) MNs. (k) Number of nerve fiber beads of *SOD1*<sup>D90A</sup> and *SOD1*<sup>D90D</sup> MNs at day 35 of differentiation. (l) Neurite density of *SOD1*<sup>D90A</sup> and *SOD1*<sup>D90D</sup> MNs at day 28 of differentiation. The nerve fiber beads are indicated by arrow heads. \*  $p < 0.05$  and \*\*  $p < 0.01$ . Scale bar, 100  $\mu\text{m}$ .

The NF<sup>+</sup> neurite density of *SOD1*<sup>G85R</sup> MNs was reduced 36% ( $21.4\% \pm 1.45\%$  of total growth area) (Figure 3b) relative to that of the *SOD1*<sup>G85G</sup> control ( $33.43\% \pm 0.84\%$  of total growth area) (Figure 3d). These data were calculated as Figure 3f. The neurite density of *SOD1*<sup>D90A</sup> MN was reduced 60% ( $9.63\% \pm 0.29\%$  of total growth area) (Figure 3h) relative to that of the *SOD1*<sup>D90D</sup> control ( $23.90\% \pm 3.05\%$  of total growth area) (Figure 3j). The data were calculated as Figure 3l. These data illustrate that we faithfully recapitulated NF aggregates in *SOD1*<sup>D90A</sup> MNs, but also discovered similar NF inclusions in *SOD1*<sup>G85R</sup> MNs for the first time. Moreover, we observed a decrease in NF<sup>+</sup> neurites in both *SOD1* mutant MNs, which could be a novel marker for quantification of ALS-related MN degeneration cytopathies in drug screening.

### 3.3. Gastrodin Reduces NF Aggregates and Promotes Nerve Fiber Extension in SOD1 ALS MNs

After the establishment of an in vitro ALS MN model with quantifiable cytopathies, we applied several natural compounds with neuroprotective effects in drug tests. Results showed that gastrodin, a major ingredient of the natural herb *Gastrodia elata* previously reported to benefit spinal cord injury [41], had therapeutic effects on ALS MNs. After 72 h of gastrodin treatment, the nerve fiber beads of *SOD1*<sup>G85R</sup> MNs (Figure 4c) were decreased but not significantly so in comparison to the control (Figure 4a; calculated as Figure 4e). However, the *SOD1*<sup>G85R</sup> MN neurite area was increased by 323% (from  $2.56\% \pm 0.16\%$  to  $8.27\% \pm 1.06\%$  of total growth area; Figure 4f) after gastrodin treatment (gastrodin: Figure 4d; control: Figure 4b).

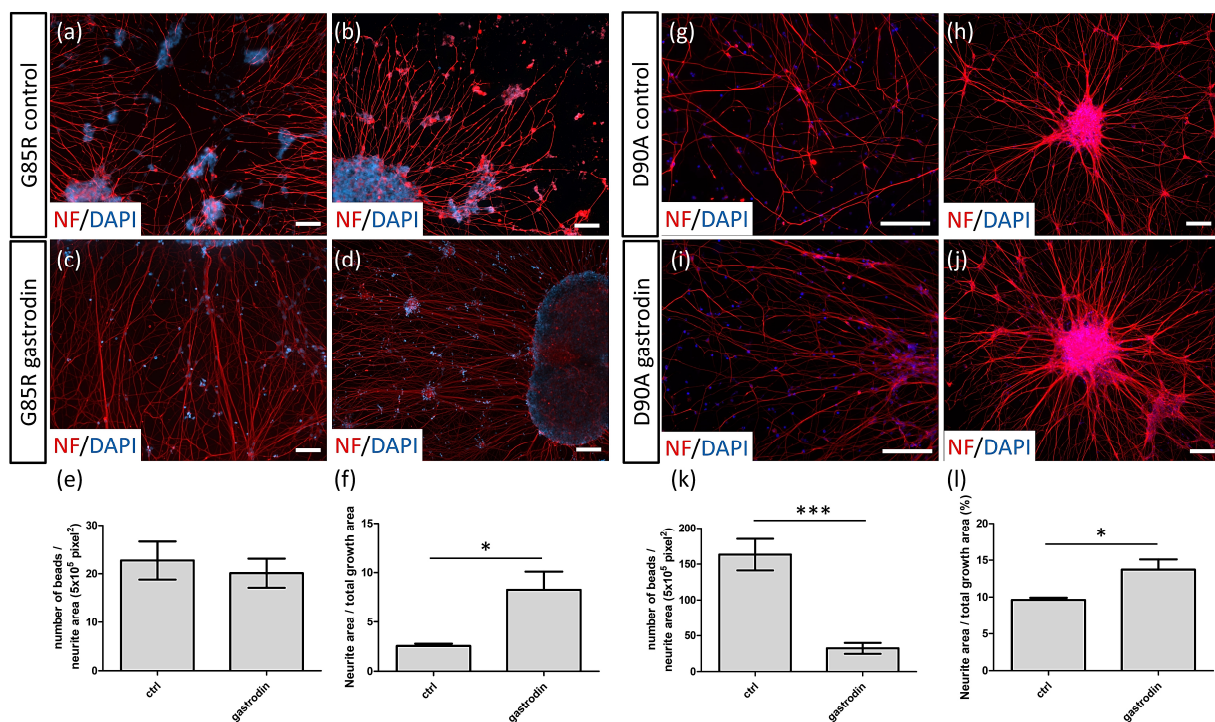


**Figure 4.** Gastrodin reduces nerve fiber abnormalities of SOD1 ALS MNs. (a–d) Nerve fiber beads (a) and neurite density (b) of untreated and gastrodin-treated *SOD1*<sup>G85R</sup> (nerve fiber beads: c; neurite density: d) MNs identified with NF immunocytochemistry staining. (e) Number of nerve fiber beads of untreated (ctrl) and gastrodin-treated *SOD1*<sup>G85R</sup> MNs at day 35 of differentiation. (f) Neurite density of untreated (ctrl) and gastrodin-treated *SOD1*<sup>G85R</sup> MNs at day 28 of differentiation. (g–j) Nerve fiber beads (g) and neurite density (h) of untreated and gastrodin-treated *SOD1*<sup>D90A</sup> (nerve fiber beads: i; neurite density: j) MNs. (k) Number of nerve fiber beads of untreated (ctrl) and gastrodin-treated *SOD1*<sup>D90A</sup> MNs at day 35 of differentiation. (l) Neurite density of untreated (ctrl) and gastrodin-treated *SOD1*<sup>D90A</sup> MNs at day 28 of differentiation. \*  $p < 0.05$ , and \*\*\*  $p < 0.001$ . Scale bar, 100  $\mu\text{m}$ .

Gastrodin also showed therapeutic effects on *SOD1*<sup>D90A</sup> nerve fiber cytopathies. After treatment, the number of NF aggregates decreased from  $163.3 \pm 12.70$  (control: Figure 4g) to  $32.38 \pm 4.39$  beads/ $5 \times 10^5$  pixels<sup>2</sup> NF (gastrodin: Figure 4i, calculated as Figure 4k). The number of nerve fiber aggregates was reversed to the basal level, similar with that of *SOD1*<sup>D90D</sup> healthy MNs ( $41.92 \pm 7.76$  beads/ $5 \times 10^5$  pixels<sup>2</sup> NF) (Figure 3k) after gastrodin treatment, illustrating the therapeutic effect of gastrodin on the NF inclusions of *SOD1*<sup>D90A</sup> MNs. Gastrodin treatment also increased *SOD1*<sup>D90A</sup> MN nerve fibers by 42.58%, from  $9.63\% \pm 0.29\%$  (control: Figure 4h) to  $13.73\% \pm 1.37\%$  of total growth area (gastrodin: Figure 4j; calculated as Figure 4l). These results support the therapeutic potential of gastrodin against both *SOD1* ALS nerve fiber phenotypes.

### 3.4. Gastrodin Reverses the Glutamate Induced Hyper-Calcium Flux in SOD1 ALS MNs

Identifying neuronal electrophysiological function markers is important for linking in vitro models with real-world ALS MN functional degeneration in patients. According to calcium image tests, *SOD1*<sup>G85R</sup> MNs showed significantly higher calcium flux ( $\Delta F/F_0$ :  $3.68 \pm 0.21$ ) than did *SOD1*<sup>G85G</sup> MNs ( $\Delta F/F_0$ :  $3.07 \pm 0.14$ ) with potassium chloride treatment but not with glutamate stimulation (Figure 5a–c). Additionally, *SOD1*<sup>D90A</sup> MNs showed higher calcium flux ( $\Delta F/F_0$ :  $7.65 \pm 1.08$ ) than did *SOD1*<sup>D90D</sup> MNs ( $\Delta F/F_0$ :  $4.26 \pm 0.23$ ) with potassium chloride treatment. After glutamate triggering, *SOD1*<sup>D90A</sup> MNs showed higher calcium influx ( $\Delta F/F_0$ :  $2.68 \pm 0.28$ ) than did *SOD1*<sup>D90D</sup> MNs ( $\Delta F/F_0$ :  $1.63 \pm 0.09$ ) (Figure 5f–h). Both *SOD1* ALS MNs expressed hyper-calcium flux to potassium ions or glutamate stimulation, which is similar to hyperexcitability cytopathy that has been reported for ALS patients [42], but this is first report from an iPSC-based model.

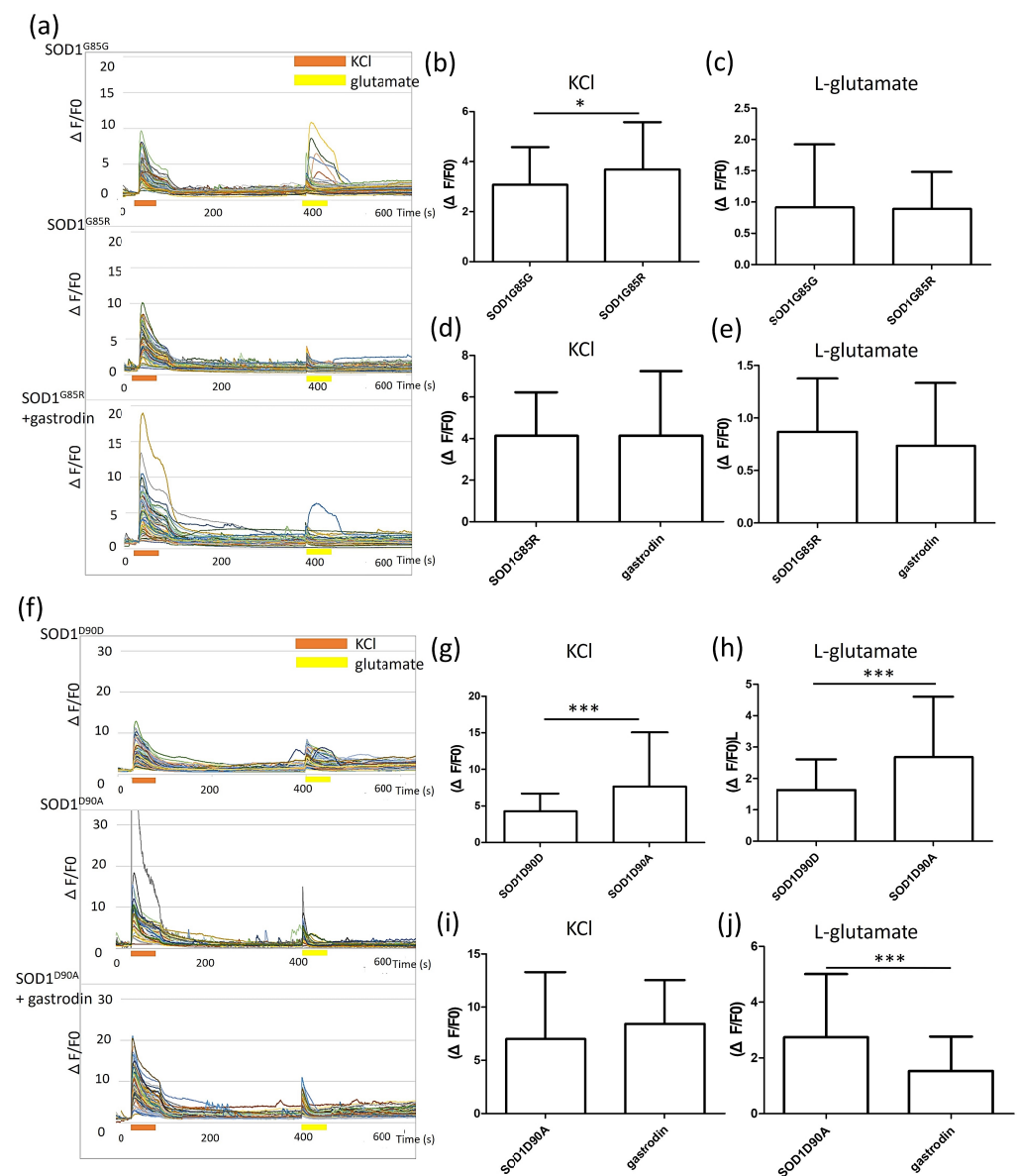


**Figure 5.** Gastrodin reverses  $SOD1^{D90A}$  MN hyper-calcium flux after glutamate stimulation. (a)  $SOD1^{G85G}$ ,  $SOD1^{G85R}$ , and gastrodin-treated  $SOD1^{G85R}$  MNs were subjected to Fluo-4 calcium imaging at day 38 of differentiation. The calcium flux stimulated by potassium chloride (presented as orange bars) and glutamate (yellow bars) was revealed with  $\Delta F/F0$ . (b,c) Average calcium flux stimulated by potassium chloride (b) and glutamate (c) of  $SOD1^{G85G}$  and  $SOD1^{G85R}$  MNs. (d,e) Average calcium flux stimulated by potassium chloride (d) and glutamate (e) of untreated and gastrodin-treated  $SOD1^{G85R}$  MNs. (f)  $SOD1^{D90D}$ ,  $SOD1^{D90A}$ , and gastrodin-treated  $SOD1^{D90A}$  MNs were subjected to calcium imaging. (g,h) Average calcium flux stimulated by potassium chloride (g) and glutamate (h) of  $SOD1^{D90D}$  and  $SOD1^{D90A}$  MNs. (i,j) Average calcium flux stimulated by potassium chloride (i) and glutamate (j) of untreated and gastrodin-treated  $SOD1^{D90A}$  MNs. \*  $p < 0.05$ , \*\*\*  $p < 0.001$ .

After gastrodin treatment, the calcium influx of  $SOD1^{D90A}$  MNs decreased from  $2.74 \pm 0.32$  to  $1.53 \pm 0.13$  after glutamate stimulation and reversed the calcium flux back to a level similar to that of  $SOD1^{D90D}$  ( $\Delta F/F0$ :  $1.63 \pm 0.09$ ) (Figure 5j). In contrast, gastrodin treatment did not alter the potassium and glutamate-induced calcium flux of  $SOD1^{G85R}$  (Figure 5d,e), or the potassium-induced calcium flux of  $SOD1^{D90A}$  MNs (Figure 5i).

### 3.5. Gastrodin Rescues Nerve Fiber Cytopathies in Sporadic ALS MNs As Well As Restoring Motor Performance and Prolonging Survival in ALS Mice

To evaluate the therapeutic potential of gastrodin in non-*SOD1*-mutated ALS MNs, PBMCs were collected from a sporadic ALS patient (sALS), i.e., without known ALS mutations on *SOD1*, *TARDBP*, *c9orf72*, *VAPB*, and *FUS*, and reprogrammed to iPSCs. sALS iPSCs presented classical pluripotent stem cell morphology (Figure 6a), normal karyotypes (Figure 6b), and pluripotent-specific markers (Figure 6c–f). According to in vitro differentiation tests, sALS iPSCs could differentiate into cell lineages with the expression of ectoderm (Figure 6g), mesoderm (Figure 6h), and endoderm (Figure 6i) progenitor markers.

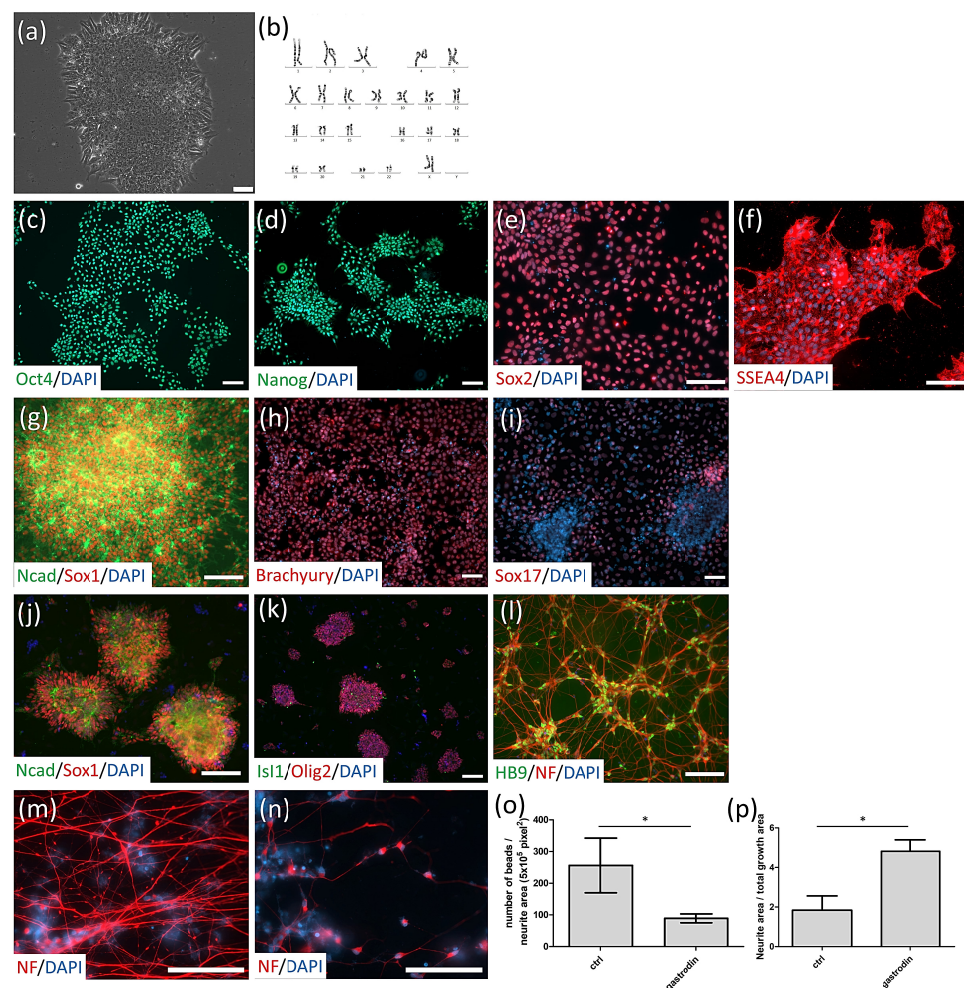


**Figure 6.** Gastrodin reverses nerve fiber degeneration in sporadic ALS MNs. (a) Morphology of sporadic ALS (sALS) iPSC clones. (b) Karyotype of sALS iPSCs. (c–f) sALS iPSC-expressed pluripotent stem cell markers including Oct-4 (c), Nanog (d), Sox-2 (e), and SSEA4 (f). (g–i) In vitro differentiation of sALS iPSCs into three germ layer cell types with markers including the ectoderm markers N-cadherin and Sox-1 (g), mesoderm marker Brachyury (h), and endoderm marker Sox-17 (i). (j–l) sALS iPSC line-derived MNs were identified with neural stem cell markers (N-cadherin and Sox-1) and MN progenitor markers (Oligo-2 and Islet-1) at day 15 of differentiation, and with an MN marker (HB9) and a neuronal marker (NF) at day 25 of differentiation. (m,n) Nerve fiber beads (m) and cell body inclusions (n) of NF protein on sALS MNs. (o,p) Number of nerve fiber beads (o) and neurite intensity (p) of untreated (ctrl) and gastrodin-treated sALS MNs at day 62 of differentiation. \*  $p < 0.05$ . Scale bar, 100  $\mu\text{m}$ .

sALS iPSCs differentiated into MNs with high efficiency. NSC markers (*sox1* and N-cadherin) and MN progenitor markers (*Islet1* and *Oligo2*) were expressed at day 15 of differentiation, whereas MN markers (*HB9* and *NF*) were expressed at day 28 (Figure 6j–l). Nerve fiber cytopathies of sALS MNs arose around day 60 of differentiation: nerve fibers showed abnormal NF aggregates on neurites (Figure 6m), inclusions on somas, and nerve fiber fragmentations (Figure 6n). After 72 h of gastrodin treatment, the number of nerve fiber beads decreased from  $256.2 \pm 49.81$  beads/ $5 \times 10^5$  pixels<sup>2</sup> NF to  $89.17 \pm 9.79$  beads/ $5 \times 10^5$  pixels<sup>2</sup> NF (Figure 6o), whereas the amount of nerve fibers increased from  $1.84\% \pm 0.51\%$  to  $4.82\% \pm 0.41\%$  of the total growth area (Figure 6p), i.e., approximately 2.6-fold that of untreated sALS MNs. These results demonstrate that gastrodin can rescue neurite cytopathies not only in *SOD1* mutants but also in sALS MNs.

*SOD1*<sup>G93A</sup> ALS mice were used to evaluate the in vivo therapeutic effects of gastrodin. Gastrodin was delivered from 60 days-of-age at 50 or 200 mg/kg by intraperitoneal injection five times per month. Results of the rotarod and paw force experiments showed that the motor function of ALS mice was significantly increased after gastrodin treatment (Figure 7a–d). The survival period was prolonged by gastrodin:  $129.67 \pm 7.57$  days to  $146.5 \pm 11.73$  (50 mg/kg) or  $140.38 \pm 10.43$  (200 mg/kg) days (both  $p < 0.05$ ; Figure 7e). Gastrodin also improved motor function [Basso–Beattie–Bresnahan (BBB) score] at 120–148 days-of-age (Figure 7f). Thus, the therapeutic effects of gastrodin on ALS were also demonstrated in an animal model.

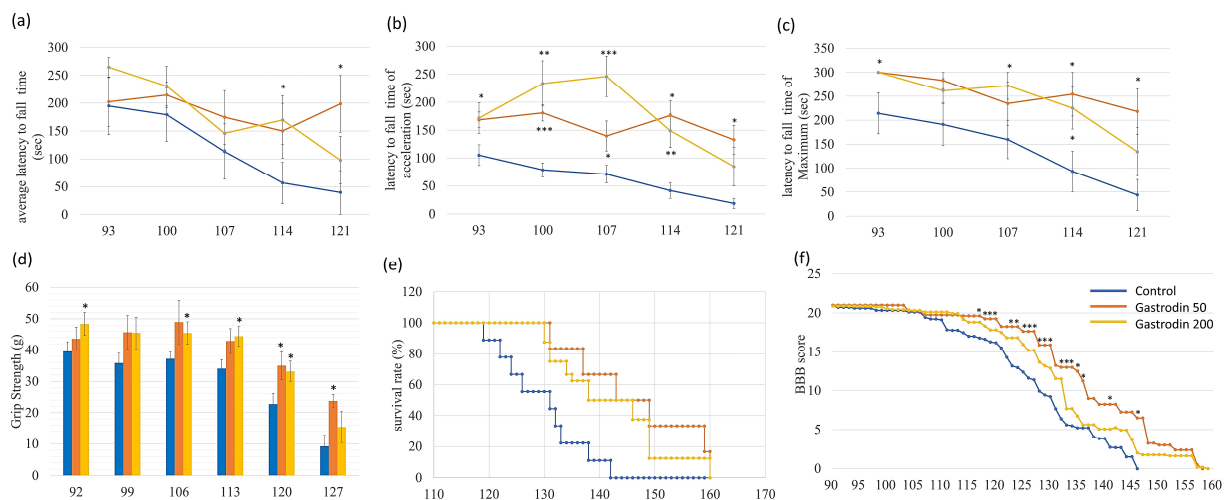


**Figure 7.** Gastrodin improves the motor function and prolongs the life span of *SOD1*<sup>G93A</sup> ALS mice. ALS mice were treated with gastrodin from 60 days of age. Data on the rotarod test (a–c), grip strength (d), survival rate (e), and BBB score (f) were recorded from 90 days-of-age. Rotarod data are presented as the average latency to fall time (a), latency to fall time of acceleration (b), and latency to fall time of maximum (c). \*  $p < 0.05$ , \*\*  $p < 0.01$ , and \*\*\*  $p < 0.001$ .

### 3.6. Gastrodin Activates the IGF-1 Signaling Pathway and GSK3 $\beta$ Activity to Rescue Nerve Fiber Cytopathies in *SOD1* ALS MNs

To elucidate the mechanism underlying the therapeutic effect of gastrodin on ALS, we employed an *SOD1*<sup>G93A</sup>-NSC34 ALS cell model with gastrodin treatment. RNA microarray results revealed that 1870 and 1812 genes were up and downregulated after gastrodin treatment (Figure 8a). Enriched genes were clustered into cell cycle, DNA repair, axon guidance, synapse functions, and signaling pathways including p53, insulin, PI3K-Akt and Ras (Figure 8b). Gene expression of most IGF-1 related downstream pathways, including the IGF-1 receptor, MAPK and PI3K-Akt signaling, were upregulated, whereas Wnt signaling was downregulated after gastrodin treatment (Figure 8c). We confirmed that GSK3 $\beta$  was activated after 2–4 h of gastrodin treatment (the phospho-GSK3 $\beta$ /GSK3 $\beta$  were  $1.67 \pm 0.12$  fold at 2 h and  $1.87 \pm 0.07$  fold at 4 h related to ctrl,  $p < 0.05$ ) (Figure 8d), consistent with Wnt pathway downregulation. The MAPK signaling pathway was activated after gastrodin treatment and P42/P44 phosphorylation of MAPK was significantly increased

after 24–48 h of treatment (the phospho-p44-MAPK/p44-MAPK were  $1.66 \pm 0.21$  fold at 24 h and  $2.11 \pm 0.46$  fold at 48 h related to ctrl,  $p < 0.05$ ; the phospho-p42-MAPK/p42-MAPK were  $2.16 \pm 0.60$  fold at 24 h and  $2.05 \pm 0.54$  fold at 48 h related to ctrl,  $p < 0.05$ ) (Figure 8d–h). The quantified protein fold changes of different time points were list below every protein group of Figure 8d and presented in Figure 8e–h.

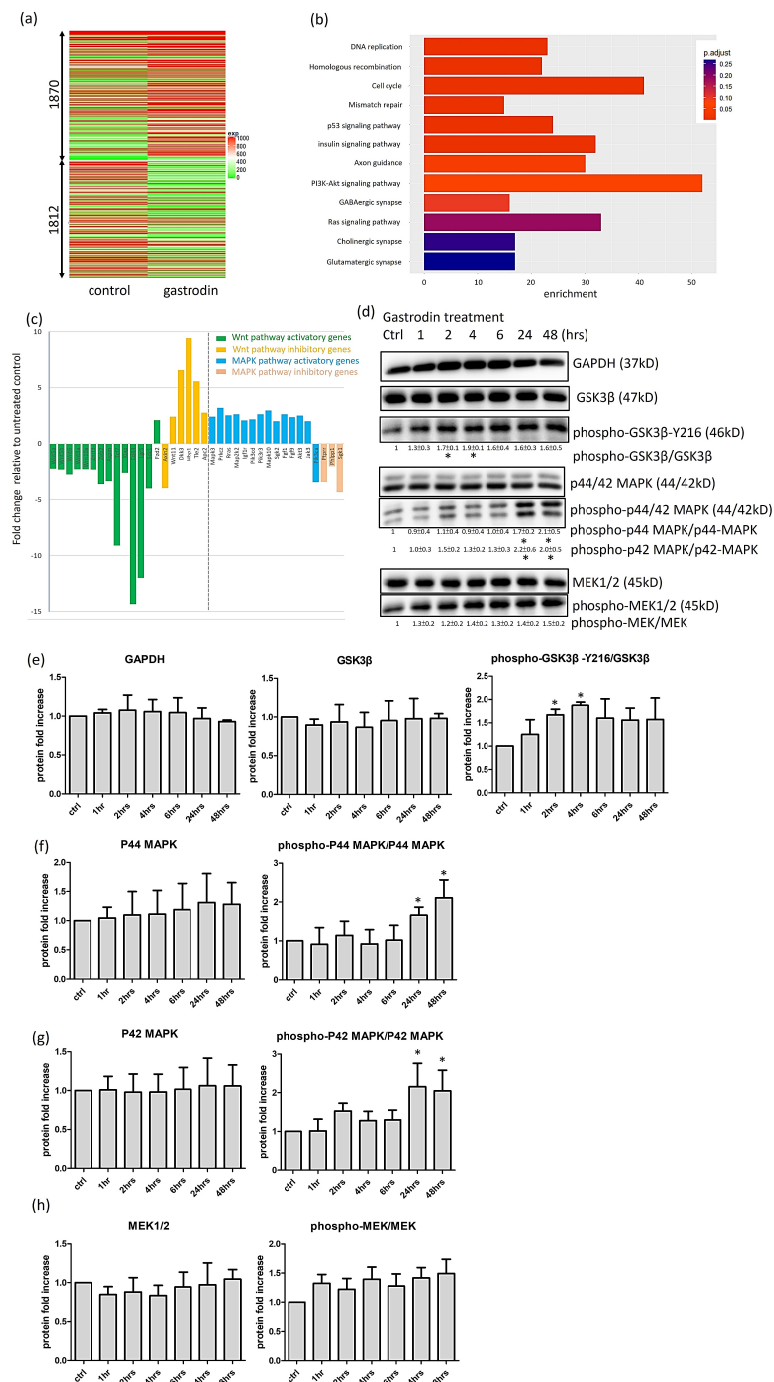


**Figure 8.** Gastrodin promotes GSK3β and MAPK pathway activation in *SOD1<sup>G93A</sup>-NSC34* MN-like cells. **(a)** Dendrogram showing clustering of gastrodin-treated and untreated *SOD1<sup>G93A</sup>-NSC34* cells based on transcriptional changes detected by RNA-microarray. **(b)** Gene sets enrichment in gastrodin-treated *SOD1<sup>G93A</sup>-NSC34* cells. **(c)** Graph of expression fold change for Wnt and MAPK signaling-related genes in gastrodin-treated and untreated control *SOD1<sup>G93A</sup>-NSC34*. **(d–h)** Western blotting of GAPDH, GSK3β, phospho-GSK3β, MAPK, phospho-MAPK, MEK, and phospho-MEK proteins from gastrodin-treated and untreated (ctrl) *SOD1<sup>G93A</sup>-NSC34* cells. \*  $p < 0.05$ .

To investigate the effect of GSK3 $\beta$  and IGF-1 coactivation on ALS therapy, *SOD1*<sup>G85R</sup> iPSC-derived MNs were treated with ligands or inhibitors of candidate signaling pathways, including Wnt3a (Wnt ligand, as an indirectly GSK3 $\beta$  inhibitor), CHIR99021 (GSK3 $\beta$  inhibitor), IWP-2 (Wnt receptor antagonist, as an indirectly GSK3 $\beta$  activator), and IGF-1. Immunofluorescence of neurite intensity showed that compared with control (Figure 9(a1)), IGF-1 (Figure 9(a5)) and IWP-2 (Figure 9(a4)) treatments enhanced ALS MN neurite growth, whereas cotreatment with IGF-1 and IWP-2 did not show additional effects compare with individual treatments (Figure 9(a7)). Wnt3a and CHIR99021 did not alter the amount of neurites in ALS MNs (Figure 9(a2,a3)), but they reversed the therapeutic function of IGF-1 (Figure 9(a6)) and showed negative effects of GSK3 $\beta$  inhibition on ALS MN neurite extension. Overall, these data were calculated as Figure 9(a8). For nerve fiber bead cytopathy, IWP-2 (Figure 9(b4)) or IGF-1 (Figure 9(b5)) treatments decreased bead number, but not significantly relative to the control (Figure 9(b1)). Cotreatment with IWP-2 and IGF-1 (Figure 9(b7)) significantly decreased the nerve fiber bead number of *SOD1*<sup>G85R</sup> ALS MNs, indicating a synergistic effect compared with that of IWP-2 or IGF-1 alone. Potentially, IWP-2 and IGF-1 cotreatment had a superior therapeutic effect on nerve fiber beads to that of gastrodin (Figure 4e). Wnt3a treatment increased nerve bead numbers (Figure 9(b2)), whereas CHIR99021 did not increase bead numbers but estimated with increased beads size (bead size estimated but not measured) (Figure 9(b3,b6)). Overall, these data were calculated as Figure 9(b8).

To evaluate the influence of GSK3 $\beta$  inhibition on the effect of gastrodin, we combined gastrodin with Wnt3a or CHIR99021 to treat MNs. With gastrodin treatment, the amount of nerve fibers significantly increased compared with that of the control (Figure 9(c2,c1)); however, compared with the effects of gastrodin alone, combined treatments with either Wnt3a (Figure 9(c4)) or CHIR99021 (Figure 9(c3)) did not significantly alter nerve fiber amounts. Thus, Wnt3a and CHIR99021 did not alter the therapeutic effect of gastrodin on nerve fiber density (Figure 9(c5)). In contrast, the number of nerve fiber beads significantly decreased after gastrodin treatment (Figure 9(d1,d2)) but re-increased after CHIR99021 (Figure 9(d3)) or Wnt3a (Figure 9(d4,d5)) cotreatment.

These results suggest that coactivation of IGF-1 and GSK3 $\beta$  could alleviate nerve fiber cytopathies and produce even better therapeutic effects than gastrodin. The addition of GSK3 $\beta$  blocker eliminates the effects of gastrodin on rescuing nerve fiber disease markers. Thus, we conclude that IGF-1 and GSK3 $\beta$  activation have positive effects on ALS therapy.

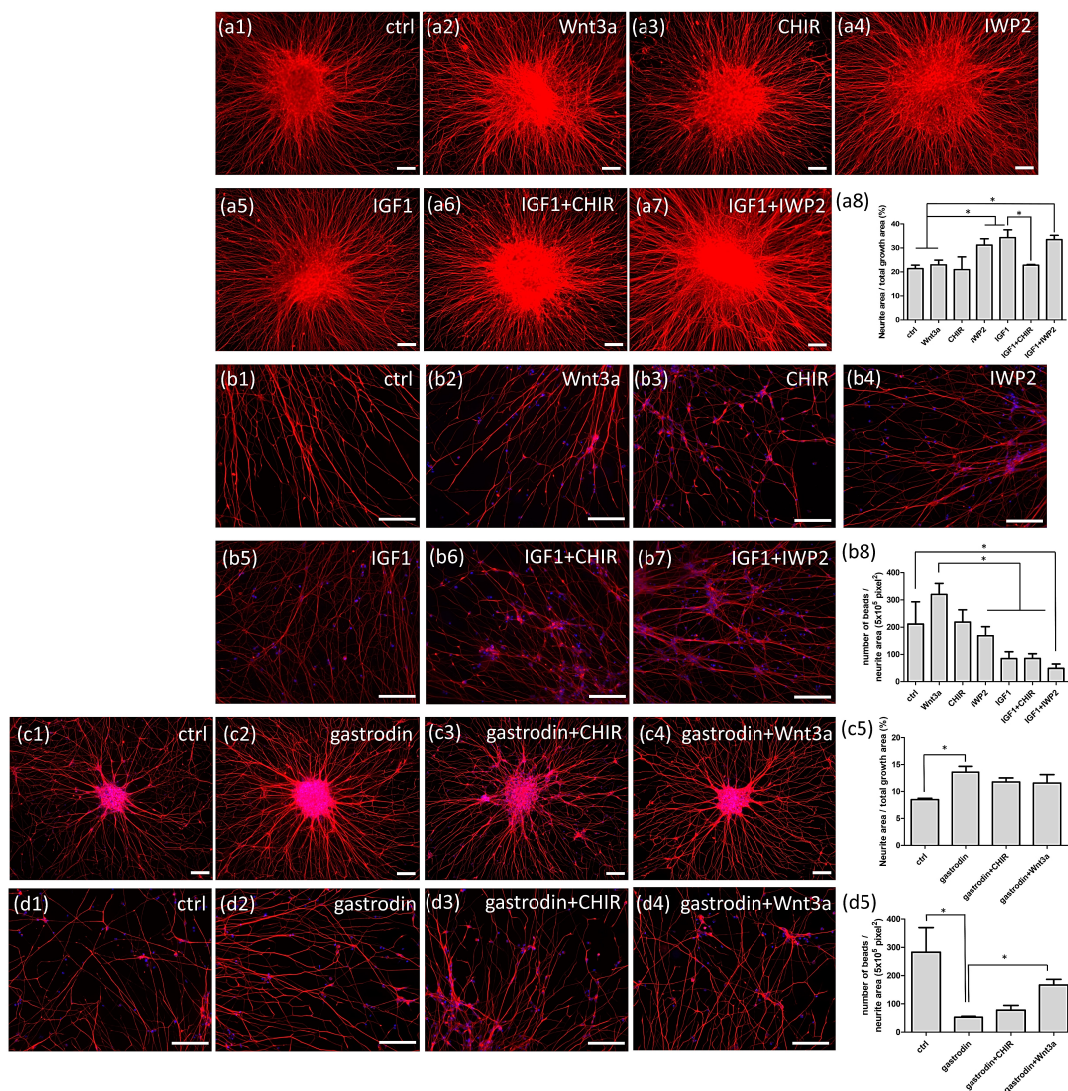


**Figure 9.** Activation of the GSK3 $\beta$  and IGF-1 pathway reduces axonal cytopathies in SOD1 mutant ALS MNs. **(a)** Neurite densities of day-28 *SOD1*<sup>G85R</sup> MNs treated with Wnt3a, CHIR99021, IWP-2, and IGF-1, and their combinations were analyzed with NF immunocytochemistry staining and calculated as **(a8)**. **(b)** Nerve fiber beads of day-35 *SOD1*<sup>G85R</sup> MNs treated with the aforementioned compounds and their combinations were analyzed and calculated as **(b8)**. **(c)** Neurite density of day-28 *SOD1*<sup>D90A</sup> MNs treated with gastrodin and its combinations with CHIR99021 or Wnt3a, were analyzed and calculated as **(c5)**. **(d)** Nerve fiber beads of day-35 *SOD1*<sup>D90A</sup> MNs treated with gastrodin and combinations were analyzed and calculated as **(d5)**. \*  $p < 0.05$ . Scale bar, 100  $\mu\text{m}$ .

#### 4. Discussion

In the present study, we modified the BiSF method [38] by replacing BIO with CHIR99021 for NSC induction and then used MN patterning based on the method of Du et al. [43]. By combining these two processes, we received ~90% of MNs from at least five ALS-related iPSC lines within 23–25 days of differentiation. Measurable nerve fiber beads and neurite degeneration cytopathies emerged within 28–38 days, confirming that this model is stable and scalable as an iPSC-based platform for ALS drug screening. We selected the candidate compound gastrodin according to its ability to improve nerve fiber cytopathies and show supportive effects on neurofunctional recovery; thus, nerve fiber phenotypes seem to be representative early-stage markers and are highly correlated with late-stage neuronal functional loss in ALS. Therefore, using early-stage nerve fiber cytopathies as first-phase screening markers before confirming with late-stage functional markers could be an effective strategy for ALS therapeutic candidate compound screening.

In neurofunctional tests of ALS MNs lasting > 60 days, we found that the hyperexcitation similar properties of *SOD1* ALS MNs arose at around day 38 of differentiation. Interestingly, in neurofunctional tests after day-60 of differentiation, both *SOD1* ALS MNs (*SOD1*<sup>G85R</sup> and *SOD1*<sup>D90A</sup>, but not *SOD1*<sup>G85G</sup> and *SOD1*<sup>D90D</sup>) triggered 488-nm fluorescence signals, which were followed by cell death immediately after glutamate treatment. Thus, hyperexcitability might worsen and finally cause MN death after normal levels of neurotransmitter stimulation in aging *SOD1* ALS MNs.

Nerve fiber beads not only presented in *SOD1*<sup>G85R</sup> and *SOD1*<sup>D90A</sup> ALS MNs but also in one sALS MN, demonstrating that nerve fiber cytopathies were not only restricted to *SOD1*-type ALS. Gastrodin treatment rescued nerve fiber beads and promoted neurite growth in sALS MNs, indicating the therapeutic potential of gastrodin on sALS.

In ALS patients and experimental animals, riluzole can prolong lifespan at the extremely late stage of disease, but it has minor effects on motor function and life quality maintenance [44,45]. Conversely, we demonstrated that the therapeutic function of gastrodin occurs largely in early-stage ALS, not only in an iPSC-based cell model but also in ALS mice. Gastrodin significantly decreased the speed of motor functional degeneration at 90 days of age and delayed the BBB score decline at 120–148 days-of-age; thus, it clearly had effects on early motor function maintenance. Consequently, combining gastrodin and riluzole may be a potential ALS therapeutic strategy worthy of further investigation.

GSK3 $\beta$  is a potential target for ALS therapy; indeed, MN samples from transgenic ALS animals express higher levels of GSK3 $\beta$  activation than normal [46]. Inhibition of GSK3 $\beta$  signaling may also benefit ALS cells or animals [47–52]. Additionally, the indirect GSK3 $\beta$  inhibitor of lithium has been applied in clinical trials [53]. However, we found that GSK3 $\beta$  played a converse role in ALS patient iPSC-derived MNs. Specifically, the inhibition of GSK3 $\beta$  by Wnt3a or CHIR99021 aggravated nerve fiber cytopathies, whereas IWP-2 treatment (an indirectly GSK3 $\beta$  activator) rescued MNs from these nerve fiber cytopathies. Interestingly, a recent study demonstrated a similar role for GSK3 $\beta$  in an *SOD1*<sup>E100G</sup> iPSC-based ALS model: Bhingre et al. (2017) found that XAV-939 (a tankyrase inhibitor, also as an indirectly GSK3 $\beta$  activator) treatment postponed the death of *SOD1*<sup>E100G</sup> MNs [33]. In another study, the overexpression of Wnt signaling-related ligands and receptors was observed in ALS patient spinal cord samples [54]. Thus, we suggest that the contrary role of GSK3 $\beta$  shown in our iPSC-based results compared with that indicated in previous non-patient-derived ALS cell or animal results demonstrates the major value of using patient cell-derived MNs as a model.

How *SOD1* mutations influence nerve fiber dynamics in ALS MNs is not yet fully clear. A previous report [27] indicated that the D90A *SOD1* protein interacts with the UTR region of NF light chain (*NF-L*) mRNA to reduce protein production, which then influences NF assembly, and finally causes ALS nerve fiber cytopathies. The shortage of *NF-L* protein expression also alters the stability and phosphorylation of *NF* heavy chain (*NF-H*) and *NF* medium chain (*NF-M*). After supplying *NF-L* with a Tet-on inducible knock-in, the researchers demonstrated a reduction in nerve fiber cytopathies. This work provided evidence to link *SOD1* mutations with ALS *NF* cytopathy. Here, we identified misfolded *SOD1* aggregates in *SOD1*<sup>G85R</sup> MNs (data not shown) but they did not colocalize with *NF* protein aggregates or inclusions, suggesting that mutant *SOD1* protein may not directly interact with *NF* protein. The phosphorylation of *NFs*, including *NF-H*, *NF-M*, and *NF-L*, plays important roles in *NF* stability, transport, and assembly, especially at phosphorylation sites on the C-terminus. MAPK and GSK3 $\beta$  are phosphate donors for essential *NF* phosphorylation [55,56]. For example, the major activation sites of *NF-H* protein are located on the proximal C-terminus. With the phosphorylation of these activation sites by GSK3 $\beta$ , MAPK, and cdk5, the *NF-H* protein switches from a closed to open configuration that is capable of transport and neurite assembly. With an inhibitory mutation (S493A) at the GSK3 $\beta$  phosphorylation site, the *NF-H* protein forms inclusions in the cell body and induces expression of *NF* aggregates and fragmented neurites [55]; this is consistent with the *SOD1* ALS MN nerve fiber cytopathies in our experiment. Thus,

apart from NF-L resupply, we speculate that activation of MAPK and GSK3 $\beta$  may rescue SOD1-induced nerve fiber phenotypes by providing sufficient phosphorylation activities at specific essential sites, which benefits NF protein transport and assembly to eliminate nerve fiber inclusions and promote neurite extension. However, the specific GSK3 $\beta$ -dependent phosphorylation sites and their antibodies on NFs must still be identified and developed.

Although both G85R and D90A *SOD1* mutant MNs had NF inclusions and degeneration cytopathies, the level of these cytopathies differed between the two lines. Compared with D90A MNs, G85R *SOD1* MNs expressed heavier nerve fiber beads, milder neurite degeneration, and less hyperexcitability, suggesting that the *SOD1* mutation site may alter the individual cytopathy levels. Evidently, further research is required to identify the mechanisms underlying the *SOD1* mutant site's effects on ALS MN cytopathies.

In addition, how gastrodin functions with the IGF-1 pathway and GSK3 $\beta$  activity is not yet clear. Indeed, the role of gastrodin in these pathways has not previously been reported. In living cells or animals, gastrodin would be converted into the secondary metabolite p-hydroxybenzyl alcohol within hours [57]; however, there is no evidence to date that p-hydroxybenzyl alcohol can promote IGF-1 or GSK3 $\beta$ . Further research should therefore be conducted to determine the working mechanisms of gastrodin.

## 5. Conclusions

In conclusion, we established a robust method by which to differentiate iPSCs into MNs (~90%). Consequently, within 38 days of differentiation, we were able to identify ALS-specific cytopathies including neurite degeneration, nerve fiber inclusions, and hyperexcitability in *SOD1* MNs that matched several clinical pathologies of patients. Although the nerve fiber beads of *SOD1*<sup>D90A</sup> MNs were previously reported by Chen et al. [27], we are the first to report them in *SOD1*<sup>G85R</sup> MNs. Moreover, both the nerve fiber degeneration and neurotransmitter hyperexcitability of *SOD1*<sup>G85R</sup> and *SOD1*<sup>D90A</sup> MNs were reported for the first time here. Gastrodin had therapeutic effects that rescued nerve fiber and neurofunctional cytopathies in ALS MNs while also improving the motor function of ALS animals. IGF-1 and GSK3 $\beta$ , both activated by gastrodin, showed therapeutic effects on nerve fiber cytopathies, demonstrating the potential of their coactivation as an ALS therapy.

**Author Contributions:** Conceptualization, S.-Z.L. and C.-Y.C.; Data curation, H.-C.T., H.-I.Y., Y.-J.T. and C.-Y.C.; Formal analysis, H.-C.T., H.-I.Y., Y.-J.T. and C.-Y.C.; Funding acquisition, H.-J.H., I.-M.C., T.-J.H., S.-Z.L. and C.-Y.C.; Investigation, H.-C.T., H.-I.Y., Y.-J.T. and C.-Y.C.; Methodology, H.-C.T., H.-I.Y., H.-L.S., X.L., M.-F.C. and C.-Y.C.; Resources, S.-Z.L.; Supervision, H.-J.H., H.-L.S., T.-W.C., S.-Z.L. and C.-Y.C.; Writing—original draft, H.-C.T., H.-I.Y., S.-Z.L. and C.-Y.C.; Writing—review & editing, H.-J.H., H.-L.S. and C.-A.L. All authors have read and agreed to the published version of the manuscript.

**Funding:** This work was financially supported by Buddhist Tzu Chi Medical Foundation (MF00A130SS01), Hualien Tzu Chi Hospital (TC-NHRI106-01 and IMAR-110-01-02) and Ministry of Science and Technology (MOST 107-2314-B-303-001-, MOST 108-2314-B-303-009-, MOST 109-2314-B-303-023-, MOST 110-2314-B-303-025- and MOST 110-2314-B-303-017-MY3), Taiwan.

**Institutional Review Board Statement:** The study was conducted according to the guidelines of the Declaration of Helsinki and with the approval of the Ethic Institutional Review Board in Hualien Tzu Chi Hospital (IRB105-131-A). All animal-related procedures were performed in accordance with the guidelines of the US National Institutes of Health and Hualien Tzu Chi Hospital (106-46), Taiwan.

**Informed Consent Statement:** Informed consent was obtained from all subjects involved in the study.

**Data Availability Statement:** Data supporting the findings of this study are available within the figures and the results section. Further data are available from the corresponding author upon reasonable request.

**Acknowledgments:** The development of high efficiency MN differentiation protocol was supported by Hong-Lin Su laboratory (Department of Life Sciences, National Chung Hsing University, Taichung, Taiwan). The authors also acknowledge the core facilities provided by the Instrument Center of Department of Medicine Research, Buddhist Tzu-Chi General Hospital and Bioinnovation Center, Buddhist Tzu Chi Medical Foundation, Hualien, Taiwan.

**Conflicts of Interest:** The authors declare no conflict of interest.

## References

1. Robberecht, W.; Philips, T. The changing scene of amyotrophic lateral sclerosis. *Nat. Rev. Neurosci.* **2013**, *14*, 248–264. [[CrossRef](#)]
2. Smith, R.; Pioro, E.; Myers, K.; Sirdofsky, M.; Goslin, K.; Meekins, G.; Yu, H.; Wymer, J.; Cudkowicz, M.; Macklin, E.A.; et al. Enhanced bulbar function in amyotrophic lateral sclerosis: The nedexta treatment trial. *Neurotherapeutics* **2017**, *14*, 762–772. [[CrossRef](#)]
3. Sawada, H. Clinical efficacy of edaravone for the treatment of amyotrophic lateral sclerosis. *Expert Opin. Pharmacother.* **2017**, *18*, 735–738. [[CrossRef](#)] [[PubMed](#)]
4. Jaiswal, M.K. Riluzole and edaravone: A tale of two amyotrophic lateral sclerosis drugs. *Med. Res. Rev.* **2019**, *39*, 733–748. [[CrossRef](#)] [[PubMed](#)]
5. Deng, H.X.; Hentati, A.; Tainer, J.A.; Iqbal, Z.; Cayabyab, A.; Hung, W.Y.; Getzoff, E.D.; Hu, P.; Herzfeldt, B.; Roos, R.P.; et al. Amyotrophic lateral sclerosis and structural defects in Cu, Zn superoxide dismutase. *Science* **1993**, *261*, 1047–1051. [[CrossRef](#)]
6. Rosen, D.R.; Siddique, T.; Patterson, D.; Figlewicz, D.A.; Sapp, P.; Hentati, A.; Donaldson, D.; Goto, J.; O'Regan, J.P.; Deng, H.-X.; et al. Mutations in Cu/Zn superoxide dismutase gene are associated with familial amyotrophic lateral sclerosis. *Nature* **1993**, *362*, 59–62. [[CrossRef](#)] [[PubMed](#)]
7. Hadano, S.; Hand, C.K.; Osuga, H.; Yanagisawa, Y.; Otomo, A.; Devon, R.S.; Miyamoto, N.; Showguchi-Miyata, J.; Okada, Y.; Singaraja, R.; et al. A gene encoding a putative GTPase regulator is mutated in familial amyotrophic lateral sclerosis 2. *Nat. Genet.* **2001**, *29*, 166–173. [[CrossRef](#)] [[PubMed](#)]
8. Neumann, M.; Sampathu, D.M.; Kwong, L.K.; Truax, A.C.; Micsenyi, M.C.; Chou, T.T.; Bruce, J.; Schuck, T.; Grossman, M.; Clark, C.M.; et al. Ubiquitinated TDP-43 in frontotemporal lobar degeneration and amyotrophic lateral sclerosis. *Science* **2006**, *314*, 130–133. [[CrossRef](#)] [[PubMed](#)]
9. Arai, T.; Hasegawa, M.; Akiyama, H.; Ikeda, K.; Nonaka, T.; Mori, H.; Mann, D.; Tsuchiya, K.; Yoshida, M.; Hashizume, Y.; et al. TDP-43 is a component of ubiquitin-positive tau-negative inclusions in frontotemporal lobar degeneration and amyotrophic lateral sclerosis. *Biochem. Biophys. Res. Commun.* **2006**, *351*, 602–611. [[CrossRef](#)] [[PubMed](#)]
10. Renton, A.E.; Majounie, E.; Waite, A.; Simon-Sanchez, J.; Rollinson, S.; Gibbs, J.R.; Schymick, J.C.; Laaksovirta, H.; van Swieten, J.C.; Myllykangas, L.; et al. A hexanucleotide repeat expansion in C9ORF72 is the cause of chromosome 9p21-linked ALS-FTD. *Neuron* **2011**, *72*, 257–268. [[CrossRef](#)]
11. Kwiatkowski, T.J., Jr.; Bosco, D.A.; Leclerc, A.L.; Tamrazian, E.; Vanderburg, C.R.; Russ, C.; Davis, A.; Gilchrist, J.; Kasarskis, E.J.; Munsat, T.; et al. Mutations in the FUS/TLS gene on chromosome 16 cause familial amyotrophic lateral sclerosis. *Science* **2009**, *323*, 1205–1208. [[CrossRef](#)]
12. Vance, C.; Rogelj, B.; Hortobagyi, T.; De Vos, K.J.; Nishimura, A.L.; Sreedharan, J.; Hu, X.; Smith, B.; Ruddy, D.; Wright, P.; et al. Mutations in FUS, an RNA processing protein, cause familial amyotrophic lateral sclerosis type 6. *Science* **2009**, *323*, 1208–1211. [[CrossRef](#)] [[PubMed](#)]
13. Maruyama, H.; Morino, H.; Ito, H.; Izumi, Y.; Kato, H.; Watanabe, Y.; Kinoshita, Y.; Kamada, M.; Nodera, H.; Suzuki, H.; et al. Mutations of optineurin in amyotrophic lateral sclerosis. *Nature* **2010**, *465*, 223–226. [[CrossRef](#)]
14. Tsuda, H.; Han, S.M.; Yang, Y.; Tong, C.; Lin, Y.Q.; Mohan, K.; Haueter, C.; Zoghbi, A.; Harati, Y.; Kwan, J.; et al. The amyotrophic lateral sclerosis 8 protein VAPB is cleaved, secreted, and acts as a ligand for Eph receptors. *Cell* **2008**, *133*, 963–977. [[CrossRef](#)] [[PubMed](#)]
15. Carpenter, S. Proximal axonal enlargement in motor neuron disease. *Neurology* **1968**, *18*, 841–851. [[CrossRef](#)] [[PubMed](#)]
16. Hirano, A.; Nakano, I.; Kurland, L.T.; Mulder, D.W.; Holley, P.W.; Saccomanno, G. Fine structural study of neurofibrillary changes in a family with amyotrophic lateral sclerosis. *J. Neuropathol. Exp. Neurol.* **1984**, *43*, 471–480. [[CrossRef](#)]
17. Smith, E.F.; Shaw, P.J.; De Vos, K.J. The role of mitochondria in amyotrophic lateral sclerosis. *Neurosci. Lett.* **2019**, *710*, 132933. [[CrossRef](#)]
18. Walker, A.K.; Atkin, J.D. Stress signaling from the endoplasmic reticulum: A central player in the pathogenesis of amyotrophic lateral sclerosis. *IUBMB Life* **2011**, *63*, 754–763. [[CrossRef](#)]
19. Barber, S.C.; Mead, R.J.; Shaw, P.J. Oxidative stress in ALS: A mechanism of neurodegeneration and a therapeutic target. *Biochim. Biophys. Acta* **2006**, *1762*, 1051–1067. [[CrossRef](#)]
20. Lutz, C. Mouse models of ALS: Past, present and future. *Brain Res.* **2018**, *1693*, 1–10. [[CrossRef](#)]
21. Morrice, J.R.; Gregory-Evans, C.Y.; Shaw, C.A. Animal models of amyotrophic lateral sclerosis: A comparison of model validity. *Neural Regen. Res.* **2018**, *13*, 2050–2054. [[CrossRef](#)]
22. Egawa, N.; Kitaoka, S.; Tsukita, K.; Naitoh, M.; Takahashi, K.; Yamamoto, T.; Adachi, F.; Kondo, T.; Okita, K.; Asaka, I.; et al. Drug screening for ALS using patient-specific induced pluripotent stem cells. *Sci. Transl. Med.* **2012**, *4*, 145ra104. [[CrossRef](#)]

23. Mitne-Neto, M.; Machado-Costa, M.; Marchetto, M.C.; Bengtson, M.H.; Joazeiro, C.A.; Tsuda, H.; Bellen, H.J.; Silva, H.C.; Oliveira, A.S.; Lazar, M.; et al. Downregulation of VAPB expression in motor neurons derived from induced pluripotent stem cells of ALS8 patients. *Hum. Mol. Genet.* **2011**, *20*, 3642–3652. [[CrossRef](#)]
24. Alves, C.J.; Dariolli, R.; Jorge, F.M.; Monteiro, M.R.; Maximino, J.R.; Martins, R.S.; Strauss, B.E.; Krieger, J.E.; Callegaro, D.; Chadi, G. Gene expression profiling for human iPSC-derived motor neurons from sporadic ALS patients reveals a strong association between mitochondrial functions and neurodegeneration. *Front. Cell. Neurosci.* **2015**, *9*, 289. [[CrossRef](#)] [[PubMed](#)]
25. Ichihyanagi, N.; Fujimori, K.; Yano, M.; Ishihara-Fujisaki, C.; Sone, T.; Akiyama, T.; Okada, Y.; Akamatsu, W.; Matsumoto, T.; Ishikawa, M.; et al. Establishment of In Vitro FUS-Associated Familial Amyotrophic Lateral Sclerosis Model Using Human Induced Pluripotent Stem Cells. *Stem Cell Reports* **2016**, *6*, 496–510. [[CrossRef](#)]
26. Imamura, K.; Izumi, Y.; Watanabe, A.; Tsukita, K.; Woltjen, K.; Yamamoto, T.; Hotta, A.; Kondo, T.; Kitaoka, S.; Ohta, A.; et al. The Src/c-Abl pathway is a potential therapeutic target in amyotrophic lateral sclerosis. *Sci. Transl. Med.* **2017**, *9*, eaaf3962. [[CrossRef](#)] [[PubMed](#)]
27. Chen, H.; Qian, K.; Du, Z.; Cao, J.; Petersen, A.; Liu, H.; Blackburn, L.W.; Huang, C.L.; Errigo, A.; Yin, Y.; et al. Modeling ALS with iPSCs reveals that mutant SOD1 misregulates neurofilament balance in motor neurons. *Cell Stem Cell* **2014**, *14*, 796–809. [[CrossRef](#)]
28. Kiskinis, E.; Sandoe, J.; Williams, L.A.; Boulting, G.L.; Moccia, R.; Wainger, B.J.; Han, S.; Peng, T.; Thams, S.; Mikkilineni, S.; et al. Pathways disrupted in human ALS motor neurons identified through genetic correction of mutant SOD1. *Cell Stem Cell* **2014**, *14*, 781–795. [[CrossRef](#)] [[PubMed](#)]
29. Burkhardt, M.F.; Martinez, F.J.; Wright, S.; Ramos, C.; Volfson, D.; Mason, M.; Garnes, J.; Dang, V.; Lievers, J.; Shoukat-Mumtaz, U.; et al. A cellular model for sporadic ALS using patient-derived induced pluripotent stem cells. *Mol. Cell. Neurosci.* **2013**, *56*, 355–364. [[CrossRef](#)]
30. Zhang, K.; Donnelly, C.J.; Haeusler, A.R.; Grima, J.C.; Machamer, J.B.; Steinwald, P.; Daley, E.L.; Miller, S.J.; Cunningham, K.M.; Vidensky, S.; et al. The C9orf72 repeat expansion disrupts nucleocytoplasmic transport. *Nature* **2015**, *525*, 56–61. [[CrossRef](#)]
31. Guo, W.; Naujock, M.; Fumagalli, L.; Vandoorne, T.; Baatsen, P.; Boon, R.; Ordovas, L.; Patel, A.; Welters, M.; Vanwelden, T.; et al. HDAC6 inhibition reverses axonal transport defects in motor neurons derived from FUS-ALS patients. *Nat. Commun.* **2017**, *8*, 1–15. [[CrossRef](#)] [[PubMed](#)]
32. Fujimori, K.; Ishikawa, M.; Otomo, A.; Atsuta, N.; Nakamura, R.; Akiyama, T.; Hadano, S.; Aoki, M.; Saya, H.; Sobue, G.; et al. Modeling sporadic ALS in iPSC-derived motor neurons identifies a potential therapeutic agent. *Nat. Med.* **2018**, *24*, 1579–1589. [[CrossRef](#)] [[PubMed](#)]
33. Bhinge, A.; Namboori, S.C.; Zhang, X.; VanDongen, A.M.J.; Stanton, L.W. Genetic correction of SOD1 mutant iPSCs reveals ERK and JNK activated AP1 as a driver of neurodegeneration in amyotrophic lateral sclerosis. *Stem Cell Rep.* **2017**, *8*, 856–869. [[CrossRef](#)] [[PubMed](#)]
34. Macarthur, C.C.; Fontes, A.; Ravinder, N.; Kuninger, D.; Kaur, J.; Bailey, M.; Taliana, A.; Vemuri, M.C.; Lieu, P.T. Generation of human-induced pluripotent stem cells by a nonintegrating RNA Sendai virus vector in feeder-free or xeno-free conditions. *Stem Cells Int.* **2012**, *2012*, 1–9. [[CrossRef](#)]
35. Basso, D.M.; Beattie, M.S.; Bresnahan, J.C. Graded histological and locomotor outcomes after spinal cord contusion using the NYU weight-drop device versus transection. *Exp. Neurol.* **1996**, *139*, 244–256. [[CrossRef](#)]
36. Bruijn, L.I.; Becher, M.W.; Lee, M.K.; Anderson, K.L.; Jenkins, N.A.; Copeland, N.G.; Sisodia, S.S.; Rothstein, J.D.; Borchelt, D.R.; Price, D.L.; et al. ALS-linked SOD1 mutant G85R mediates damage to astrocytes and promotes rapidly progressive disease with SOD1-containing inclusions. *Neuron* **1997**, *18*, 327–338. [[CrossRef](#)]
37. Cao, X.; Antonyuk, S.V.; Seetharaman, S.V.; Whitson, L.J.; Taylor, A.B.; Holloway, S.P.; Strange, R.W.; Doucette, P.A.; Valentine, J.S.; Tiwari, A.; et al. Structures of the G85R variant of SOD1 in familial amyotrophic lateral sclerosis. *J. Biol. Chem.* **2008**, *283*, 16169–16177. [[CrossRef](#)]
38. Chen, S.-M.; Lee, M.-S.; Chang, C.-Y.; Lin, S.-Z.; Cheng, E.-H.; Liu, Y.-H.; Pan, H.-C.; Lee, H.-C.; Su, H.-L. Prerequisite OCT4 maintenance potentiates the neural induction of differentiating human embryonic stem cells and induced pluripotent stem cells. *Cell Transplant.* **2015**, *24*, 829–844. [[CrossRef](#)]
39. Chang, C.-Y.; Chen, S.-M.; Lu, H.-E.; Lai, S.-M.; Lai, P.-S.; Shen, P.-W.; Chen, P.-Y.; Shen, C.-I.; Harn, H.-J.; Lin, S.-Z.; et al. N-butyridenephthalide attenuates Alzheimer’s disease-like cytopathy in Down syndrome induced pluripotent stem cell-derived neurons. *Sci Rep.* **2015**, *5*, 8744. [[CrossRef](#)] [[PubMed](#)]
40. Maury, Y.; Come, J.; Piskorowski, R.A.; Salah-Mohellibi, N.; Chevalyere, V.; Peschanski, M.; Martinat, C.; Nedelec, S. Combinatorial analysis of developmental cues efficiently converts human pluripotent stem cells into multiple neuronal subtypes. *Nat. Biotechnol.* **2015**, *33*, 89–96. [[CrossRef](#)] [[PubMed](#)]
41. Du, F.; Wang, X.; Shang, B.; Fang, J.; Xi, Y.; Li, A.; Diao, Y. Gastrodin ameliorates spinal cord injury via antioxidant and anti-inflammatory effects. *Acta Biochim. Pol.* **2016**, *63*, 589–593. [[CrossRef](#)]
42. Bae, J.S.; Simon, N.G.; Menon, P.; Vucic, S.; Kiernan, M.C. The puzzling case of hyperexcitability in amyotrophic lateral sclerosis. *J. Clin. Neurol.* **2013**, *9*, 65–74. [[CrossRef](#)]
43. Du, Z.W.; Chen, H.; Liu, H.; Lu, J.; Qian, K.; Huang, C.L.; Zhong, X.; Fan, F.; Zhang, S.C. Generation and expansion of highly pure motor neuron progenitors from human pluripotent stem cells. *Nat. Commun.* **2015**, *6*, 1–9. [[CrossRef](#)] [[PubMed](#)]

44. Gurney, M.E.; Fleck, T.J.; Himes, C.S.; Hall, E.D. Riluzole preserves motor function in a transgenic model of familial amyotrophic lateral sclerosis. *Neurology* **1998**, *50*, 62–66. [[CrossRef](#)] [[PubMed](#)]
45. Hogg, M.C.; Halang, L.; Woods, I.; Coughlan, K.S.; Prehn, J.H.M. Riluzole does not improve lifespan or motor function in three ALS mouse models. *Amyotroph. Lateral Scler. Front. Degener.* **2018**, *19*, 438–445. [[CrossRef](#)] [[PubMed](#)]
46. Warita, H.; Manabe, Y.; Murakami, T.; Shiro, Y.; Nagano, I.; Abe, K. Early decrease of survival signal-related proteins in spinal motor neurons of presymptomatic transgenic mice with a mutant SOD1 gene. *Apoptosis* **2001**, *6*, 345–352. [[CrossRef](#)] [[PubMed](#)]
47. Allodi, I.; Comley, L.; Nichterwitz, S.; Nizzardo, M.; Simone, C.; Benitez, J.A.; Cao, M.; Corti, S.; Hedlund, E. Differential neuronal vulnerability identifies IGF-2 as a protective factor in ALS. *Sci. Rep.* **2016**, *6*, 25960. [[CrossRef](#)]
48. Shin, J.H.; Cho, S.I.; Lim, H.R.; Lee, J.K.; Lee, Y.A.; Noh, J.S.; Joo, I.S.; Kim, K.W.; Gwag, B.J. Concurrent administration of Neu2000 and lithium produces marked improvement of motor neuron survival, motor function, and mortality in a mouse model of amyotrophic lateral sclerosis. *Mol. Pharmacol.* **2007**, *71*, 965–975. [[CrossRef](#)]
49. Sugai, F.; Yamamoto, Y.; Miyaguchi, K.; Zhou, Z.; Sumi, H.; Hamasaki, T.; Goto, M.; Sakoda, S. Benefit of valproic acid in suppressing disease progression of ALS model mice. *Eur. J. Neurosci.* **2004**, *20*, 3179–3183. [[CrossRef](#)]
50. Feng, H.-L.; Leng, Y.; Ma, C.-H.; Zhang, J.; Ren, M.; Chuang, D.-M. Combined lithium and valproate treatment delays disease onset, reduces neurological deficits and prolongs survival in an amyotrophic lateral sclerosis mouse model. *Neuroscience* **2008**, *155*, 567–572. [[CrossRef](#)]
51. Koh, S.-H.; Kim, Y.; Kim, H.Y.; Hwang, S.; Lee, C.H.; Kim, S.H. Inhibition of glycogen synthase kinase-3 suppresses the onset of symptoms and disease progression of G93A-SOD1 mouse model of ALS. *Exp. Neurol.* **2007**, *205*, 336–346. [[CrossRef](#)]
52. Li, B.; Xu, W.; Luo, C.; Gozal, D.; Liu, R. VEGF-induced activation of the PI3-K/Akt pathway reduces mutant SOD1-mediated motor neuron cell death. *Brain Res. Mol. Brain Res.* **2003**, *111*, 155–164. [[CrossRef](#)]
53. Group, U.K.-L.S.; Morrison, K.E.; Dhariwal, S.; Hornabrook, R.; Savage, L.; Burn, D.J.; Khoo, T.K.; Kelly, J.; Murphy, C.L.; Al-Chalabi, A.; et al. Lithium in patients with amyotrophic lateral sclerosis (LiCALS): A phase 3 multicentre, randomised, double-blind, placebo-controlled trial. *Lancet Neurol.* **2013**, *12*, 339–345. [[CrossRef](#)]
54. Gonzalez-Fernandez, C.; Gonzalez, P.; Andres-Benito, P.; Ferrer, I.; Rodriguez, F.J. Wnt signaling alterations in the human spinal cord of amyotrophic lateral sclerosis cases: Spotlight on Fz2 and Wnt5a. *Mol. Neurobiol.* **2019**, *56*, 6777–6791. [[CrossRef](#)]
55. Vohnoutka, R.B.; Boumil, E.F.; Liu, Y.; Uchida, A.; Pant, H.C.; Shea, T.B. Influence of a GSK3beta phosphorylation site within the proximal C-terminus of Neurofilament-H on neurofilament dynamics. *Biol. Open* **2017**, *6*, 1516–1527. [[CrossRef](#)] [[PubMed](#)]
56. Lee, S.; Pant, H.C.; Shea, T.B. Divergent and convergent roles for kinases and phosphatases in neurofilament dynamics. *J. Cell Sci.* **2014**, *127*, 4064–4077. [[CrossRef](#)] [[PubMed](#)]
57. Lin, L.-C.; Chen, Y.-F.; Lee, W.-C.; Wu, Y.-T.; Tsai, T.-H. Pharmacokinetics of gastrodin and its metabolite p-hydroxybenzyl alcohol in rat blood, brain and bile by microdialysis coupled to LC-MS/MS. *J. Pharm. Biomed. Anal.* **2008**, *48*, 909–917. [[CrossRef](#)] [[PubMed](#)]